NIST Technical Note 1836

Effect of Acoustic Excitation on R134a/Al_2O_3 Nanolubricant Mixture Boiling on a Reentrant Cavity Surface with Extensive Measurement and Analysis Details

Mark A. Kedzierski
Steven E. Fick

http://dx.doi.org/10.6028/NIST.TN.1836

National Institute of Standards and Technology
U.S. Department of Commerce

NIST Technical Note 1836

Effect of Acoustic Excitation on R134a/Al_2O_3 Nanolubricant Mixture Boiling on a Reentrant Cavity Surface with Extensive Measurement and Analysis Details

Mark A. Kedzierski
Energy and Environment Division
Engineering Laboratory

Steven E. Fick
Semiconductor and Dimensional Metrology Division
Physical Measurement Laboratory

This publication is available free of charge from:
http://dx.doi.org/10.6028/NIST.TN.XXXX

July 2014

U.S. Department of Commerce
Penny Pritzker, Secretary

National Institute of Standards and Technology
Willie May, Under Secretary of Commerce for Standards and Technology and Director

National Institute of Standards and Technology Technical Note 1836
Natl. Inst. Stand. Technol. Tech. Note 1836, 41 pages (July 2014)
CODEN: NTNOEF

This publication is available free of charge from:
http://dx.doi.org/10.6028/NIST.TN.1836

This publication is available free of charge from: http://dx.doi.org/10.6028/NIST.TN.1836

Effect of Acoustic Excitation on R134a/Al_2O_3 Nanolubricant Mixture Boiling on a Reentrant Cavity Surface with Extensive Measurement and Analysis Details

M. A. Kedzierski and S. E. Fick
National Institute of Standards and Technology
Gaithersburg, MD 20899

ABSTRACT

This paper quantifies the influence of acoustic excitation of Al_2O_3 nanoparticles on the pool boiling performance of R134a/polyolester mixtures on a commercial (Turbo-BII-HP) boiling surface. A nanolubricant with 10 nm diameter Al_2O_3 nanoparticles at a 5.1 % volume fraction in the base polyolester lubricant was mixed with R134a at a 1 % mass fraction. The study showed that high frequency ultrasound at 1 MHz can improve R134a/nanolubricant boiling on a reentrant cavity surface by as much as 44 %. This maximum enhancement occurred for an applied power level to the fluid of approximately 6 W and a heat flux of approximately 6.9 kW/m^2. Applied power levels larger and smaller than 6 W resulted in smaller boiling heat transfer enhancements. In total, five different applied power levels were studied: 0 W, 4 W, 6 W, 8 W, and 12 W. The largest and smallest enhancement averaged over the tested heat flux range was approximately 12 % and 2 % for applied power levels of 6 W and 4 W, respectively. In-situ insonation at 1 MHz resulted in an improved dispersion of the nanolubricant on the test surface. An existing pool boiling model for refrigerant/nanolubricant mixtures was modified to include the effect of acoustic excitation. For heat fluxes greater than 25 kWm^{-2}, the model was within 4.5 % of the measured heat flux ratios for mixtures at all applied power levels. The average agreement between measurements and predictions was approximately 1 % for all power levels.

Keywords: acoustics, additives, aluminum oxide, boiling, enhanced heat transfer, nanolubricant, nanotechnology, refrigerants, refrigerant/lubricant mixtures, structured surface, ultrasound

TABLE OF CONTENTS

LIST OF FIGURES

LIST OF TABLES

This publication is available free of charge from: http://dx.doi.org/10.6028/NIST.TN.1836

INTRODUCTION

For nearly a century, it has been known that ultrasound can be used to create bubbles via cavitation and/or influence the motion of bubbles or of the fluid for physical or chemical benefit (Leong et al., 2011). More recently, the interaction between nanoparticles and bubbles have resulted in measureable enhancement of the boiling heat transfer of refrigerant/lubricant mixtures (Kedzierski, 2011, 2012a). The enhancement of refrigerant boiling with nanolubricants (lubricants with nanoparticles) is mainly due to an exchange of momentum between the nanoparticles and the bubbles (Kedzierski, 2011, 2012a). The purpose of the present study was to determine if refrigerant/nanolubricant boiling could be further enhanced with acoustic excitation based on the premise that the ultrasound would contribute to the exchange of momentum between nanoparticles and bubbles.

There are far more boiling studies of acoustic enhancement of neat fluids like water and refrigerant than there are for nanofluids, and even fewer studies with refrigerant/nanolubricant mixtures. A review article by Legay et al. (2011) identified sixteen acoustically enhanced boiling studies, only two of which were for nanofluids, while no refrigerant/nanolubricant studies were cited. In addition, the present authors were unable to find another acoustically enhanced refrigerant/nanolubricant boiling study in the open literature. Nevertheless, there is good reason to believe that ultrasound can improve refrigerant/nanolubricant boiling heat transfer. For example, Kim et al. (2004) showed that the pool boiling heat flux for FC-72 on a wire can be increased by approximately 133 % by exciting the test fluid with 48 kHz from a piezoelectric transducer spaced 10 mm to 40 mm below the heated wire. They attributed the enhancement to "the reduction of bubble size departing the heating wire and to the acoustic streaming sweeping the bubbles over the heating wire." Riley (1998) showed that acoustic streaming is driven by Reynolds stresses that result in stokeslet to jet-like fluid flow. These incompressible flows take place in the main body of the fluid and act on all things in it including, presumably, bubbles and nanoparticles. Thus, gradients in momentum flux, as caused by acoustic streaming, are likely to increase the exchange of momentum between nanoparticles and bubbles resulting in improved boiling heat transfer. This line of reasoning is by no means new. For example, ultrasound was used in the first half of the last century by Wood and Loomis (1927) to move particles in oil in order to induce flocculation.

Bonekamp and Bier (1997) also realized a 90 % increase in the pool boiling heat transfer coefficient on a smooth tube for mixtures of R32 and R134a and attributed the improvement to "better mixing in the liquid boundary near the heating wall." They also show that the enhancement is not as pronounced for larger boiling heat fluxes due to the absorption of the ultrasound in the greater bubble density associated with larger boiling heat fluxes. Conversely, Zhou et al. (2002) observed an increase in the boiling heat transfer of acetone with increasing heat flux for fixed acoustic excitation. They attribute the boiling enhancement to "cavitation bubbles providing nucleated embryos to the boiling surface." Heffington and Glezer (2004) describe an observed 425 % boiling enhancement by ultrasound as caused by bubbles being ejected from the surface in a jet-like formation. The above research demonstrates both the complexity of the effect and the potential benefit of ultrasound on boiling.

Zhou and Liu (2004) have shown that even when nanoparticles, in the absence of lubricant, fail to enhance the boiling of fluids, acoustic excitation can enhance the boiling heat transfer of an acetone nanofluid by as much as 38 %. Zhou and Liu (2004) claim that the enhancement is due in part to the ultrasound keeping the calcium carbonate nanoparticles from filling boiling cavities and by activating "smaller vapor embryos." For boiling of refrigerant/nanolubricants, the lubricant excess layer that resides on the boiling surface keeps the nanoparticles suspended in Brownian motion and prevents them from filling the boiling cavities (Kedzierski, 2011). Consequently, part of the 38 % increase observed by Zhou and Liu (2004) would not have been realized had the acetone nanofluid been dilutely mixed with lubricant. For this reason, the resulting acoustic enhancement of boiling refrigerant/nanolubricants may not be as large as 38 %. Zhou (2004) performed an acetone nanofluids study similar to the aforementioned, but with copper nanoparticles rather than calcium carbonate. Zhou (2004) observed as much as a 52 % enhancement of the nanofluid boiling with ultrasound excitation.

Studies by Henderson et al. (2010), Bi et al. (2007), Peng et al. (2011), Hu (2013), and Kedzierski (2009) have explored the use of nanolubricants as a means for improving efficiencies of air-conditioning and refrigeration equipment. For low flow qualities, Henderson et al. (2010) have shown that CuO nanoparticles can improve the flow boiling heat transfer of refrigerant/lubricant mixtures by as much as 76 % and that the lubricant can act as a necessary dispersant. Peng et al. (2010) have shown that diamond nanolubricants can improve refrigerant/lubricant pool boiling by as much as 63 %. Similarly, copper-oxide nanoparticles have also been shown to improve refrigerant/lubricant pool boiling by as much as 245 % (Kedzierski and Gong, 2009). These preceding studies suggest that it is worth investigating the potential benefits of acoustic excitation of nanolubricants for large commercial chillers.

Consequently, the scope of the present investigation was to determine if refrigerant/nanolubricant boiling on a reentrant cavity type surface could be enhanced by acoustic excitation. With externally mounted transducers of the type and resonance frequencies typically used in ultrasonic cleaners, tens of watts of acoustic excitation can be achieved easily. However, for the associated wavelengths (e.g., approximately 12 mm at 50 kHz), a spherical sound wave would be generated that could not be focused near the test section. A uniform plane wave parallel and above the entire length of the test section was achieved by choosing a wavelength that was significantly smaller than the diameter of the transducer. For this task, a 1 MHz transducer with a nominal circular active area 14 mm in diameter, and a near field zone length of 8 cm in the R134a/nanolubricant mixture was chosen. The single internal transducer assembly excites a cylindrical volume of fluid parallel to the horizontal, flat, copper, Turbo BII HP (commercial) finned surface. For liquid R134a at the saturated test temperature, the acoustic wavelength is approximately 0.6 mm.

To achieve the above scope, boiling tests of a R134a/nanolubricant mixture at four ultrasound power levels were made on the horizontal, flat, copper, Turbo-BII-HP-finned surface. A commercial polyolester lubricant (RL68H)[1] with a nominal kinematic viscosity of 72.3 $\mu m^2/s$ at 313.15 K was the base lubricant that was mixed with nominally 10 nm diameter

Al_2O_3 nanoparticles. Al_2O_3 nanoparticles have the advantages of a well-established, successful dispersion technology and being relatively inert with respect to lubricated compressor parts.

TEST FLUIDS

A manufacturer used a proprietary surfactant at a mass of 6.2 % of the mass of the Al_2O_3 as a dispersant for the RL68H/Al_2O_3 mixture (nanolubricant). The manufacturer made the mixture such that approximately 24.7 % of the mass was Al_2O_3 particles. From this mixture, a nanolubricant with a 16.7 % mass fraction of Al_2O_3 was made by adding neat RL68H and ultrasonically mixing the solution for approximately 24 h. The 16.7 % Al_2O_3 mass fraction in the nanolubricant corresponds to a volume fraction (ϕ) of 5.1 %. In this study, the 5.1 % volume fraction nanolubricant is identified as 5AlO. The R134a/5AlO (99/1) mixture produced a nanoparticle surface density of the lubricant excess layer, N_{np}/A_s (Kedzierski, 2012a), of approximately 2.8 x 10^{20} m^{-2}. The value of N_{np}/A_s was calculated assuming that all of the nanoparticles charged to the test rig reside uniformly distributed on the heat transfer surface.

Boiling tests with the refrigerant/5AlO (99/1) mixture with increasing acoustic excitation power were designed to determine the effect of ultrasound power level on the boiling. The applied power levels (P_a) were nominally 4 W, 6 W, 8 W, and 12 W. In addition, the boiling heat transfer of R134a/5AlO (99/1) mixture without acoustic excitation ($P_a = 0$) was measured to serve as a baseline for comparison to the tests with excitation.

APPARATUS

Figure 1 shows a schematic of the apparatus that was used to measure the pool boiling data of this study. More specifically, the apparatus was used to measure the liquid saturation temperature (T_s), the average pool-boiling heat flux (q''), and the wall temperature (T_w) of the test surface. The three principal components of the apparatus were the test chamber, the condenser, and the purger. The internal dimensions of the test chamber were 25.4 mm × 257 mm × 1.54 m. The test chamber was charged with approximately 7 kg of refrigerant, giving a liquid height of approximately 80 mm above the test surface. As shown in Fig. 1, the test section was visible through two opposing, flat 150 mm × 200 mm quartz windows. The bottom of the test surface was heated with high velocity (2.5 m/s) water flow. The vapor produced by liquid boiling on the test surface was condensed by the brine-cooled, shell-and-tube condenser and returned as liquid to the pool by gravity. Also visible through the window, as shown in Fig. 1, is the ultrasonic piezoelectric transducer. Figure 2 shows the transducer and its theoretical 8 cm near field zone. The beam axis is parallel to and approximately 23 mm above the boiling surface. Further details of the test apparatus can be found in Kedzierski (2002) and Kedzierski (2001).

The ultrasonic transducer was a cylindrical assembly approximately 25 mm in diameter and 51 mm long. It was attached to the end of a length of nominally 8 mm diameter tubing supported by a compression fitting at the top of the test tank. Ultrasonic output was taken from the circular active area, nominally 14 mm in diameter, of a disc-shaped piezoelectric element that constitutes the end face of the transducer. The piezoelectric element was air-backed, made of Type 4 lead zirconate titanate, and designed to operate at 1 MHz. The sinusoidal radiofrequency (RF) drive signal was provided by a 100 W power amplifier driven

by a function generator set to 1.0 MHz, the measured resonance frequency of the transducer. The power level applied to the fluid was measured using an RF power meter interposed in the feedline linking the power amplifier and the transducer. The reflected power was also measured and used to calculate the net power (P_n) absorbed by the fluid by subtracting it from the applied power. The net power was nominally 1.9 W, 3.6 W, 5.4 W, and 7.7 W for the 4 W, 6 W, 8 W, and 12 W applied power levels, respectively. The net power along with the surface area of the transducer was used to calculate a net acoustic intensity (I_n) of approximately 12.3 kWm^{-2}, 23.4 kWm^{-2}, 35.1 kWm^{-2}, and 50.0 kWm^{-2} for the applied power levels 4 W, 6 W, 8 W, and 12 W, respectively.

TEST SURFACE

Figure 3 shows the oxygen-free high-conductivity (OFHC) copper flat test plate used in this study. The test plate was machined out of a single piece of OFHC copper by electric discharge machining (EDM). The internal fins of a commercial 25 mm (outer-diameter) Turbo-BII-HP tube were removed by EDM. The tube was then cut axially, annealed, flattened, and soldered onto the top of the test plate. Figure 4 shows a photograph of the fin surface. The Turbo-BII-HP has approximately 826 fins per meter (fpm) oriented along the short axis of the plate. The overall height and tip-width of a fin are 0.76 mm and 0.36 mm, respectively.

MEASUREMENTS AND UNCERTAINTIES

The standard uncertainty is the positive square root of the estimated variance. The individual standard uncertainties are combined to obtain the expanded uncertainty (U), which is calculated from the law of propagation of uncertainty with a coverage factor. All measurement uncertainties are reported at the 95 % confidence level except where specified otherwise. For the sake of brevity, only a summary of the basic measurements and uncertainties is given below. Complete detail on the heat transfer measurement techniques and uncertainties can be found in Kedzierski (2000) and Appendix A, respectively.

A Dynamic Light Scattering (DLS) technique was used to measure the average nanoparticle size on a number basis. The diameter of most of the particles (D_{np}) was approximately 10 nm (10.1 nm ± 1.3 nm) and the particles were well dispersed in the lubricant (Kedzierski, 2010). Figure 5 shows a Transmission Electron Microscopy (TEM) image of the nanoparticles as taken by Sarkas (2009). The image confirms the good dispersion and shows that the particles are spherical with most of them having diameters of approximately 10 nm or less and a few having diameters close to 50 nm.

All of the copper-constantan thermocouples and the data acquisition system were calibrated against a glass-rod standard platinum resistance thermometer (SPRT) and a reference voltage to a residual standard deviation of 0.005 K. Considering the fluctuations in the saturation temperature during the test and the standard uncertainties in the calibration, the expanded uncertainty of the average saturation temperature was no greater than 0.04 K. Consequently, it is estimated that the expanded uncertainty of the temperature measurements was less than 0.1 K.

Twenty 0.5 mm diameter thermocouples were force fitted into the wells of the side of the test plate shown in Fig. 3. The heat flux and the wall temperature were obtained by regressing the measured temperature distribution of the block to the governing two-dimensional conduction equation (Laplace equation). In other words, rather than using the boundary conditions to solve for the interior temperatures, the interior temperatures were used to solve for the boundary conditions following a backward stepwise procedure given in Kedzierski (1995)[1]. As shown in Fig. 3, the origin of the coordinate system was centered on the surface with respect to the y-direction at the heat transfer surface. Centering the origin in the y-direction reduced the uncertainty of the wall heat flux and temperature calculations by reducing the number of fitted constants involved in these calculations.

Fourier's law and the fitted constants from the Laplace equation were used to calculate the average heat flux (q'') normal to and evaluated at the heat transfer surface based on its projected area. The average wall temperature (T_w) was calculated by integrating the local wall temperature (T). The wall superheat was calculated from T_w and the measured temperature of the saturated liquid (T_s). Considering this, the relative expanded uncertainty in the heat flux ($U_{q''}$) was greatest at the lowest heat fluxes, approaching 9 % of the measurement near 10 kW/m^2. In general, the $U_{q''}$ remained approximately between 3 % and 7 % for heat fluxes greater than 20 kW/m^2. The average random error in the wall superheat (U_{Tw}) remained mainly between 0.06 K and 0.08 K with an average value of approximately 0.07 K. Plots of $U_{q''}$ and U_{Tw} versus heat flux can be found in Appendix A.

EXPERIMENTAL RESULTS

The heat flux was varied between approximately 10 kW/m^2 and 120 kW/m^2 to simulate a range of possible operating conditions for R134a chillers. All pool-boiling measurements were made at 277.6 K saturated conditions. The data were recorded consecutively starting at the largest heat flux and descending in intervals of approximately 4 kW/m^2. The descending heat flux procedure minimized the possibility of any hysteresis effects on the data, which would have made the data sensitive to the initial operating conditions. Table 2 presents the measured heat flux and wall superheat for all the data of this study. Table 3 gives the number of test days and data points for each fluid. A total of 952 measurements were made over 49 days.

The test fluid was prepared by charging the test chamber (see Fig. 1) with pure R134a of a known mass. Next, a measured mass of nanolubricant or lubricant was injected with a syringe through a port in the test chamber. The refrigerant/lubricant solution was mixed by flushing pure refrigerant through the same port where the lubricant was injected. All compositions were determined from the masses of the charged components and are given on a mass fraction basis. The maximum uncertainty of the lubricant mass fraction (x_b) measurement is approximately 0.02 %, e.g., the range of a 1.0 % mass fraction is between 0.98 % and 1.02 %. The nominal or target mass composition is used in the discussion. For example, the “actual” mass composition of the RL68H in the R134a/5AlO (99/1) mixture was 1.00 % ± 0.02 %.

[1] Table 1 provides functional forms of the Laplace equation that were used in this study in the same way as was done in Kedzierski (1995) and in similar studies by this author.

Figure 6 is a plot of the measured boiling heat flux of the refrigerant/nanolubricant (q''_{np}) versus the measured wall superheat (T_w - T_s = ΔT_s) for the Turbo-BII-HP at a saturation temperature of 277.6 K for tests with no applied acoustic excitation (P_a = 0 W). The open circles represent the measured data while the solid line is a cubic best-fit regression or estimated means of the data. Four days of P_a = 0 boiling R134a/5ALO (99/1) produced 194 measurements over a period of approximately one week. Seven of the 194 measurements were removed before fitting because they were identified as "outliers" based on having both high influence and high leverage (Belsley et al., 1980). The data sets for each test fluid presented in this manuscript exhibited a similar number of outliers and were regressed in the same manner. Table 4 gives the constants for the cubic regression of the superheat versus the heat flux for all of the fluids tested here. The residual standard deviation of the regressions – representing the proximity of the data to the mean – are given in Table 5 and are, on average, approximately 0.05 K. The dashed lines to either side of the mean represent the lower and upper 95 % simultaneous (multiple-use) confidence intervals for the mean and are, for the most part, concealed by the data symbols. From the confidence intervals, the expanded uncertainty of the estimated mean wall superheat was, on average, 0.03 K. Table 6 provides the average magnitude of the 95 % multi-use confidence interval for the fitted wall superheat for all of the test data.

The P_a = 0 measurements serve as a baseline for comparison to the R134a/5ALO (99/1) measurements that are acoustically excited. "Break-in" data had to be taken in order to remove the effect of the quality of the nanoparticle dispersion on the boiling heat transfer. Kedzierski (2012b) showed that a refrigerant/nanolubricant with well dispersed nanoparticles leads to better boiling heat transfer than for mixtures with poorer dispersed nanoparticles. This is illustrated in Fig. 6 by comparing the present measurements for R134a/5ALO (99/1) with no ultrasound excitation to those taken by Kedzierski (2013) for identical test conditions: the same test apparatus, the same test surface, and the same test fluid. Essentially, the nanoparticle dispersion improved with excitation over eight days of testing. As a result of the improving dispersion, the boiling curve moved incrementally to the left after each test day. The P_a = 0 boiling curve became repeatable, presumably, once the quality of the dispersion no longer was improved by acoustic excitation. A clearer illustration of the effect of improved nanolubricant dispersion is shown in Fig. 7. Figure 7 plots the ratio of the R134a/5ALO (99/1) mixture heat flux after extended sonication to the heat flux prior to sonication (q''_{np} /q''_{pe}) versus the pre-excitation heat flux (q''_{pe}) at the same wall superheat. On average, sonication improved the boiling heat flux by approximately 15 %.

Figure 8 is a plot of the acoustically excited measured heat flux (q''_{ae}) versus the measured wall superheat (T_w - T_s) for the R134a/5ALO (99/1) mixture at a saturation temperature of 277.6 K for five different acoustically net power levels: 0 W, 1.9 W, 3.6 W, 5.4 W, and 7.7 W. Comparison of the mean boiling curves shows that the superheats for all the excitation levels are within 0.5 K of each other for the entire tested heat flux. For all power levels, acoustic excitation has enhanced the pool boiling heat transfer relative to that for no acoustic excitation.

A more precise illustration of the effect of ultrasound on the boiling heat transfer is given in Fig. 9. Figure 9 plots the ratio of the heat flux for R134a/5ALO (99/1) with incident ultrasound excitation to the heat flux for R134a/5ALO (99/1) without excitation (q''_{ae}/q''_{np}) versus the heat flux without excitation (q''_{np}) at the same wall superheat. Figure 9 illustrates the influence of ultrasound power on the R134a/5ALO (99/1) boiling curve with solid and dashed lines representing the mean heat flux ratios for each mixture and shaded regions showing the 95 % multi-use confidence level for each mean. A heat transfer degradation exists where the heat flux ratio is less than one and the 95 % simultaneous confidence intervals (depicted by the shaded regions) do not include the value one. Figure 9 shows that no heat transfer degradations were observed as caused by the ultrasound for the entire heat flux range for the R134a/5ALO (99/1) mixture. The smallest enhancement occurred for the smallest excitation power of 4 W, which had an average heat flux ratio of approximately 1.02 between the heat fluxes of 20 kW/m^2 and 95 kW/m^2. The largest heat flux ratio, 1.44 ± 0.08, occurred for an intermediate net power level of 3.6 W at a heat flux of approximately 6.9 kW/m^2. Averaged over the entire heat flux test range, the enhancement for the 3.6 W net power level was approximately 12 %. In general, the heat flux ratio for all excitation levels was relatively constant for heat fluxes larger than 20 kW/m^2. The average measured heat flux ratio (q''_{ae}/q''_{np}), between roughly 20 kW/m^2 and 95 kW/m^2, was approximately 1.1, 1.07, and 1.04 for nominal net power levels of 3.6 W, 5.4 W, and 7.7 W, respectively.

DISCUSSION/MODEL DEVELOPMENT

The following describes the development of a pool boiling model to predict the combined nanoparticle agitation and acoustic streaming effects. The refrigerant/nanolubricant boiling theory developed in Kedzierski (2012a) is modified here to predict the acoustic excitation of nanoparticles. While a Collier's (1981) suppression model was used to predict the effect of acoustic streaming on the nanolubricant pool boiling:

$$S = \frac{q''_c}{q''} = \frac{1}{\left(1 + 2.56\times10^{-6}\,\mathrm{Re}_s^{1.17}\right)} \tag{1}$$

Here the suppression factor, S, is the ratio of the boiling heat flux with convection (q") to that without convection. Because the face of the acoustic transducer is perpendicular to the boiling surface, the streaming jet-flow induced by the acoustic transducer is parallel to the surface. The streaming Reynolds number (Re_s) is calculated from the net acoustic scattering intensity (I_n) as:

$$\mathrm{Re}_s = \frac{0.175\rho_l u_s L}{\mu_l} = \frac{0.175\rho_l L}{\mu_l}\sqrt{\frac{2I_n}{\rho_l c_l}} \tag{2}$$

Pure liquid refrigerant properties were used to calculate the Reynolds number based on the length of the plate (L). The liquid properties of the refrigerant were the density (ρ_l), the dynamic viscosity (μ_l), and the speed of sound (c_l). The 0.175 factor in eq. (2) accounts for the decay of the centerline streaming velocity (u_s) to the velocity near surface ($\bar{u}$) of the test plate, 20 mm from the jet-centerline. Görtler's (1942) analysis of a circular jet was used:

$$\frac{\overline{u}}{u_c} = \left[1 + \left(\frac{\alpha y}{2x}\right)^2\right]^{-2} \tag{3}$$

Here, y and x are the perpendicular and parallel coordinate distances, respectively, measured from the origin that is located at the center of the face of the transducer. In order to improve the fit of eq. (1) to the measurements, a flow constant, α, of approximately 6.0 was used instead of the traditional value of 13.5 or the more recent value of 11 (Schetz and Fuhs, 1999). It is likely that the presence of the bubbles in the jet flow resulted in the need for a modified α. Using the modified α in eq. (3) produced a velocity ratio of 0.175 when y and x were set to $L/2$ and 20 mm, respectively.

Sound reaches the top of the plate surface by scattering from the field of bubbles that resides above the heat transfer surface. It was assumed that the net scattering intensity (I_n) was proportional to the number of bubbles per unit surface area (N_b/A) as follows:

$$I_n = \frac{K_1 \mu_l^2 c_l}{\rho_l} \frac{N_b}{A} \tag{4}$$

where K_1 is a dimensionless constant having a value of approximately 0.43.

Only a portion (f) of the scattered sound makes its way to the boiling cavities of the surface because the cavity openings are 1/8th of the surface area, and liquid is sometimes present at the cavity opening. When liquid is at the cavity opening, it blocks the sound because the 0.6 mm wavelength of the sound in liquid is four times larger than the approximately 0.15 mm wide cavity opening. Only when vapor is at the cavity opening can sound find its way to the cavity because its wavelength (0.15 mm) is comparable to the approximate width of the cavity opening. Consequently, the scattering intensity is reduced by f in order to determine the nanoparticle velocity. The f is grouped with other unknown constants into a single constant for the model.

Equation 5 gives the boiling heat transfer model for refrigerant/aluminum oxide nanolubricant mixtures: (Kedzierski, 2012c):

$$\frac{q''_{np}}{q''_{PL}} = 1 + \frac{1.45\times10^{-9}[\mathrm{s\cdot m^{-1}}] \left.\dfrac{N_{np}}{A_s}\right|_G \sigma \nu_L \rho_v x_b}{D_{np}\left(q''_n\right)^{3/2} \rho_L \left(\rho_{np} - \rho_L\right) g (1 - x_b)^2} \tag{5}$$

where q''_n is equal to q''_{PL} normalized by 1 $\mathrm{Wm^{-2}}$. Properties included in eq. (1) are the refrigerant surface tension (σ), the refrigerant vapor density (ρ_v), the neat lubricant liquid density (ρ_L) and liquid kinematic viscosity (ν_L), and the nanoparticle density (ρ_{np}).

Equation 5 can be applied to a plain, a rectangular-finned, or the Turbo-BII-HP surface by choosing the appropriate surface geometry dependent nanoparticle surface density; $(N_{np}/A_s)_G$. The $(N_{np}/A_s)_G$ for the Turbo-BII-HP is (Kedzierski, 2013):

$$\left.\frac{N_{\mathrm{np}}}{A_{\mathrm{s}}}\right|_{\mathrm{G}} = 4.15\times10^{8}\left(q_{\mathrm{n}}^{"}\right)^{2.53}\left(\frac{N_{\mathrm{np}}}{A_{\mathrm{s}}}\cdot1\times10^{-20}\right)^{1.47} + 0.00017q_{\mathrm{n}}^{"} \tag{6}$$

The model above is based on the assumption that the enhancement is due to surface work on bubbles as caused by momentum transfer between growing bubbles and nanoparticles suspended within the lubricant excess layer. The $N_{\mathrm{np}}/A_{\mathrm{s}}$ is obtained by calculating the entire active surface area of the evaporator (A_{s}) and dividing it into the total number of nanoparticles (N_{np}) charged to the evaporator, which can be obtained by assuming a spherical particle diameter of an average size.

The re-derivation of eq. (5) can be tailored to acoustic excitation by starting with its fundamental governing equation, which is a momentum balance between a colliding nanoparticle and bubble:

$$\frac{\Delta M_{\mathrm{b}}}{M_{\mathrm{bi}}}+1=1+\frac{N_{\mathrm{np}}M_{\mathrm{np}}\Delta u_{\mathrm{np}}}{N_{\mathrm{b}}M_{\mathrm{bi}}u_{\mathrm{bi}}} \tag{7}$$

The masses of the nanoparticle (M_{np}) and the bubble before impact (M_{bi}) are calculated from the density of the nanoparticle (ρ_{np}) and the refrigerant vapor (ρ_{v}), respectively, while assuming a spherical shape. The change in velocity of the nanoparticle (Δu_{np}) after impact with the bubble can be represented using the coefficient of restitution (e) as done in Beer and Johnston (1977):

$$\Delta u_{\mathrm{np}} = (1+e)\left(u_{\mathrm{np}}-u_{\mathrm{b}}\right) \tag{8}$$

Here the bubble velocity is assumed to be constant and to remain unchanged by the impact so that the energy exchange is in the form of surface work on the bubble, which is responsible for the boiling enhancement. The constant e becomes part of a group of constants that was determined from the regression of the complete model to the measured boiling heat flux. The number of bubbles (N_{b}) was obtained from eq. (4).

The ratio of the acoustically enhanced refrigerant/nanolubricant boiling heat flux ($q_{\mathrm{ae}}^{"}$) to the refrigerant/nanolubricant boiling heat flux without acoustic enhancement ($q_{\mathrm{np}}^{"}$) is the sum of the nanoparticle effects from eq. (7) and the suppression effects from eq. (1):

$$\frac{q_{\mathrm{ae}}^{"}}{q_{\mathrm{np}}^{"}}=\frac{\Delta M_{\mathrm{b}}}{M_{\mathrm{bi}}}+1+S-1=\frac{N_{\mathrm{np}}M_{\mathrm{np}}\Delta u_{\mathrm{np}}}{N_{\mathrm{b}}M_{\mathrm{bi}}u_{\mathrm{bi}}}+S \tag{9}$$

Substitution of the previously described parameters into eq. (9) and regressing with the boiling measurements to obtain the constants yields:

This publication is available free of charge from: http://dx.doi.org/10.6028/NIST.TN.1836

$$\frac{q''_{ae}}{q''_{np}} = 0.353\frac{N_{np}}{A_s}\frac{D_{np}^4\rho_{np}c_l\mu_l^2}{\rho_v\rho_l D_b^3\mu_L c_L\,\mathrm{Re}_{np}}\left[\left(\frac{12832}{c_L}\right)-\frac{\rho_L D_{np}}{\mu_L\,\mathrm{Re}_{np}}\right]+\frac{1}{\left(1+2.56\times10^{-6}\,\mathrm{Re}_s^{1.17}\right)} \quad (10)$$

where c_L is the speed of sound in the lubricant.

The nanoparticle Reynolds number Re_{np} is calculated as:

$$\mathrm{Re}_{np} = \frac{\rho_L u_{np} D_{np}}{\mu_L} = \frac{\rho_L D_{np}}{\mu_L}\sqrt{\frac{2I_n}{\rho_L c_L}} \quad (11)$$

The bubble diameter is calculated from the refrigerant/lubricant pool-boiling model of Kedzierski (2003):

$$\frac{D_b}{2} = \frac{0.75 l_a \rho_L (1-x_b)}{x_b\rho_v} = \frac{18.75[\text{Å}]\rho_L(1-x_b)}{x_b\rho_v} \quad (12)$$

where x_b is the mass fraction of the lubricant in the bulk mixture, and the l_a represents the thickness of the lubricant excess layer that is removed by a departing bubble and is taken as two monolayers, which is approximately 25 Å for lubricant. Equation (12) is valid for $x_b > 0$.

Figure 10 compares the acoustically enhanced refrigerant/nanolubricant boiling predictions of eq. (10) to the measured means for the 5AlO (99/1) mixture. For heat fluxes greater than 25 $\mathrm{kWm^{-2}}$, the predictions are within ± 2 % of the measured means for the 4 W, 6 W, and 8 W power levels. The average underprediction for the 4 W and 6 W was approximately 0.8 % and 0.4 %, respectively. The average overpredition for the 8 W power level was approximately 0.8 %. The boiling measurements for the 12 W power level were underpredicted by no more than 4.5 %, with an average underprediction of 1 %, for heat fluxes greater than 25 $\mathrm{kWm^{-2}}$.

Figure 11 illustrates the effect of the net power level on the acoustically obtained boiling enhancement for the R134a/nanolubricant mixture. Equation 10 was used to produce the solid line that shows the maximum boiling enhancement occurs near a net power level of approximately 3.6 W. According to the model, increases in the net power past 3.6 W caused an increasing of the acoustic streaming and corresponding suppression of boiling, which leads to a decrease in the boiling enhancement. Net power levels less than 3.6 W have sufficiently small streaming velocities to negate the agitating effect of the ultrasound on the nanoparticles. Consequently, as the net power is increased from 1.9 W to 3.6 W the enhancement also becomes larger. Measured means for a q''_{np} of approximately 30 $\mathrm{kWm^{-2}}$ are plotted as circles for the various power levels. The agreement with the model is shown to be within 1 % for this condition.

Future research is required to verify the effect of the distance and orientation of the acoustic transducer on the acoustic streaming. In addition, the scattering of the sound from the bubbles needs to be better understood along with how the sound interacts with the boiling

surface. This additional work would include direct quantification of f; the fraction of I_n that reaches the boiling cavities.

CONCLUSIONS

The effect of acoustic excitation on the boiling performance of a R134a/nanolubricant on a flattened, horizontal Turbo-BII-HP was investigated. A nanolubricant containing roughly 10 nm diameter Al_2O_3 nanoparticles at 5.1 % volume fraction with a polyolester lubricant was mixed with R134a to a 1 % mass fraction. The study showed that acoustic excitation can improve R134a/nanolubricant boiling on a Turbo-BII-HP, thus demonstrating that the boiling performance of reentrant cavity surfaces can be enhanced if a sufficient acoustic excitation is provided. For example, applied power levels of 4 W, 6 W, 8 W, and 12 W produced average boiling enhancements of 2 %, 10 %, 7 %, and 4 %, respectively. The study also illustrated the importance of a having a sufficiently dispersed nanolubricant for improved boiling heat transfer.

A model was developed to predict the effects of acoustic excitation on R134a/nanolubricant boiling on the Turbo-BII-HP surface. The model accounts for acoustic streaming effects and the nanoparticle agitation by the ultrasound. An existing model for predicting refrigerant/nanolubricant boiling was modified to model the interaction between the nanoparticles and the bubbles, while a suppression factor was used to model the acoustic streaming effects. For heat fluxes greater than 25 kWm^{-2}, the model is within 4.5 % of the measured heat flux for all acoustic power levels. The average agreement between measurements and predictions was approximately 1 % for all power levels. The model predicts and optimum power level that is a consequence of the balance between increasing nanoparticle-bubble interaction and convective suppression with increasing acoustic power.

ACKNOWLEDGEMENTS

This work was funded by the U.S. Department of Energy (project no. DE-EE0002057/004) under Project Managers Antonio Bouza and Bahman Habibzadeh. Thanks go to Junemo Koo of Kyung Hee University and to the following NIST personnel for their constructive criticism of the draft manuscript: A. Persily, and P. Domanski. Furthermore, the author extends appreciation to W. Guthrie and A. Heckert of the NIST Statistical Engineering Division for their consultations on the uncertainty analysis. Boiling heat transfer measurements were taken by D. Wilmering of Dakota Consulting Inc. at the NIST laboratory. The RL68H (EMKARATE RL 68H) was donated by K. Lilje of CPI Engineering Services, Inc. The RL68H1AlO was manufactured by Nanophase Technologies with an aluminum oxide and dispersant in RL68H especially for NIST.

NOMENCLATURE

English Symbols

A_n	regression constant in Table 4 n=0,1,2,3
A_s	heat transfer surface area, m
c	speed of sound, $m \cdot s^{-1}$
D_{np}	nanoparticle diameter, m
e	coefficient of restitution
f	fraction of I_n that reaches boiling cavities
I_n	acoustic scattering intensity, $W \cdot m^{-2}$
L	test surface length shown in Fig. 3, m
M	mass, kg
N_b	number of bubbles
N_{np}	number of nanoparticles
N_{np}/A_s	nanoparticle surface density, m^{-2}
P_a	applied power level to acoustic transducer, W
P_n	net power level from acoustic transducer, W
q''	average wall heat flux, $W \cdot m^{-2}$
q''_n	$= \frac{q''_{PL}}{1W \cdot m^{-2}}$
Re_s	streaming Reynolds number given by eq. (2)
S	suppression factor given by eq. (1)
T	temperature, K
T_w	temperature at roughened surface, K
u	velocity, $m \cdot s^{-1}$
U	expanded uncertainty
X	model terms given in Table 1
x_b	bulk lubricant mass fraction

Greek symbols

α	flow constant given in eq. (3)
ΔT_s	wall superheat: T_w - T_s, K
μ	dynamic viscosity, $kg \cdot m^{-1} \cdot s^{-1}$
ν	kinematic viscosity, $m^2 \cdot s^{-1}$
σ	surface tension of refrigerant, $N \cdot m^{-1}$
ρ	density, $kg \cdot m^{-3}$
ϕ	nanoparticle volume fraction

English Subscripts

ae	acoustically enhanced/excited
Al	R134a/nanolubricant mixture
bi	bubble before impact
G	surface geometry dependent
l	liquid refrigerant
L	pure lubricant without nanoparticles
nL	nanolubricant
np	nanoparticle/with nanoparticles

p	pure R134a
PL	refrigerant/pure lubricant (R134a/RL68H) mixture
q"	heat flux
s	saturated state, streaming
Tw	wall temperature
v	refrigerant vapor

REFERENCES

Beer, F. P., and Johnston, E. R., 1977, Vector Mechanics for Engineers: Dynamics, McGraw-Hill, New York, 3rd ed., pp. 594-598.

Belsley, D. A., Kuh, E., and Welsch, R. E., 1980, Regression Diagnostics: Identifying Influential Data and Sources of Collinearity, New York: Wiley.

Bi, S., Shi, L., and Zhang, L., 2007, "Performance Study of a Domestic Refrigerator Using R134a/Mineral Oil/Nano-TiO_2 as Working Fluid," *Proceedings of International Conference of Refrigeration,* Beijing, ICRO7-B2-346.

Bonekamp, S., and Bier, K., 1997, "Influence of Ultrasound on Pool Boiling Heat Transfer to Mixtures of the Refrigerants R23 and R134a," Int. J. Refrig., Vol. 20, No. 8, pp. 606-615.

Collier, J. G., 1981, "Forced Convective Boiling," in Two-Phase Flow and Heat Transfer in the Power and Process Industries, A. E. Bergles, J. G. Collier, J. M. Delhaye, G. F. Hewitt, and F. Mayinger, Eds., Hemisphere, New York, pg. 250.

Görtler, H., 1942, "," Z Angew Math Mech, Vol. 22, pp. 244-254.

Heffington, S., and Glezer, A., 2004, "Enhanced Boiling Heat Transfer by Submerged Ultrasonic Vibrations," Proceedings of the Therminic 2004, Sophia Antipolis, France.

Henderson, K., Park, Y., Liu, L., Jacobi, A. M., 2010, "Flow-Boiling Heat Transfer of R-134a-Based Nanofluids in a Horizontal Tube," IJHMT, 53, 944-951

Hu, H., Peng, H., and Ding, G., 2013,"Nucleat Pool Boiling Heat Transfer Characteristics of Refrigerant/Nanolubricant Mixture with Surfactant," Int. J. Refrigeration, Vol. 36, pp. 1045-1055.

Kedzierski, M. A., 2013, "Effect of Concentration on R134a/Al2O3 Nanolubricant Mixture Boiling on a Reentrant Cavity Surface with Extensive Measurement and Analysis Details," NIST Technical Note 1813, U.S. Department of Commerce, Washington, D.C.

Kedzierski, M. A., 2012a, "R134a/Al2O3 Nanolubricant Mixture Boiling on a Rectangular Finned Surface," ASME J. Heat Transfer, Vol. 134, 121501.

Kedzierski, M. A., 2012b, "Effect of Diamond Nanolubricant on R134a Pool Boiling Heat Transfer," ASME Journal of Heat Transfer, Vol. 134, 051001.

Kedzierski, M. A., 2011, "Effect of Al_2O_3 Nanolubricant on R134a Pool Boiling Heat Transfer," Int. J. Refrigeration, Vol. 34, pp. 498-508.

Kedzierski, M. A., 2010, "Effect of Al_2O_3 Nanolubricant on a Passively Enhanced R134a Pool Boiling Surface with Extensive Measurement and Analysis Details," NIST Technical Note 1677, U.S. Department of Commerce, Washington, D.C.

Kedzierski, M. A., 2009, "Effect of CuO Nanoparticle Concentration on R134a/Lubricant Pool-Boiling Heat Transfer," ASME J. Heat Transfer, Vol. 131, No. 4, 043205.

Kedzierski, M. A., and Gong, M., 2009, "Effect of CuO Nanolubricant on R134a Pool Boiling Heat Transfer with Extensive Measurement and Analysis Details," Int. J. Refrigeration, Vol. 25, pp. 1110-1122.

Kedzierski, M. A., 2003, "A Semi-Theoretical Model for Predicting R123/Lubricant Mixture Pool Boiling Heat Transfer," Int. J. Refrigeration, Vol. 26, pp. 337-348.

Kedzierski, M. A., 2002, "Use of Fluorescence to Measure the Lubricant Excess Surface Density During Pool Boiling," Int. J. Refrigeration, Vol. 25, pp. 1110-1122.

Kedzierski, M. A., 2001, "Use of Fluorescence to Measure the Lubricant Excess Surface Density During Pool Boiling," NISTIR 6727, U.S. Department of Commerce, Washington, D.C.

Kedzierski, M. A., 2000, "Enhancement of R123 Pool Boiling by the Addition of Hydrocarbons," Int. J. Refrigeration, Vol. 23, pp. 89-100.

Kedzierski, M. A., 1995, "Calorimetric and Visual Measurements of R123 Pool Boiling on Four Enhanced Surfaces," NISTIR 5732, U.S. Department of Commerce, Washington.

Kim, H. Y., Kim, Y. G., and Kang, B. H., 2004, "Enhancement of Natural Convection and Pool Boiling Heat Transfer Via Ultrasonic Vibration," I J of Heat and Mass Transfer, Vol. 47, No. 12-13, pp. 2831–2840.

Legay, M., Gondrexon, N., Le Person, S., Boldo, P., and Bontemps, A., 2011, "Enhancement of Heat Transfer by Ultrasound: Review and Recent Advances," I. J. Chem. Eng., Vol. 2011, 670108.

Leong, T., Ashokkumar, M., and Kentish, S., 2011, "The Fundamentals of Power Ultrasound– A Review," Acoustics Australia, Vol. 39, No. 2, pp. 54-63.

Peng, H., Ding, G., Hu, H., and Jiang, W., 2011, "Effect of Nanoparticle Size on Nucleate Pool Boiling Heat Transfer of Refrigerant/oil Mixture with Nanopartilces," Int. J. Heat and Mass Transfer, Vol. 54, pp. 1839-1850.

Peng, H., Ding, G., Hu, H., Jiang, W., Zhuang, D., and Wang, K., 2010, "Nucleate Pool Boiling Heat Transfer Characteristics of Refrigerant/oil Mixture with Diamond Nanopartilces," Int. J. Refrigeration, Vol. 33, pp. 347-358.

Riley, N., 1998, "Acoustic Streaming," Theoret. Comput. Fluid Dynamics, Vol. 10, pp. 349-356.

Sarkas, H., 2009, Private Communications, Nanophase Technologies Corporation, Romeoville, IL.

Schetz, J. A., and Fuhs, A. E., 1999, Fundamentals of Fluid Mechanics, J. Wiley, New York, p. 427.

Wood, R.W., and Loomis, A., L., 1927, "The Physical and Biological Effects of High-Frequency Sound-Waves of Great Intensity," Philosophical Magazine and Journal of Science, Series 7, Vol. 4, No. 22, pp. 417-436.

Zhou, D. W., 2004, "Heat Transfer Enhancement of Copper Nanofluid with Acoustic Cavitation," I. J. Heat and Mass Trans, Vol. 47, pp. 3109-3117.

Zhou, D. W., and Liu, D-Y., 2004, "Heat Transfer Characteristics of Nanofluids in an Acoustic Cavitation Field," Heat Transfer Engineering, Vol. 25, No. 6, pp. 54-61.

Zhou, D. W., Liu, D. Y., Hu, X. G., and Ma, C. F., 2002, "Effect of Acoustic Cavitation on Boiling Heat Transfer," Experimental Thermal and Fluid Science, Vol. 26, pp. 931-938.

This publication is available free of charge from: http://dx.doi.org/10.6028/NIST.TN.1836

Table 1 Conduction model choice

X_0= constant (all models) X_1= x X_2= y X_3= xy $X_4=x^2-y^2$ $X_5= y(3x^2-y^2)$ $X_6= x(3y^2-x^2)$ $X_7= x^4+y^4-6(x^2)y^2$ $X_8= yx^3-xy^3$	
Fluid	Most frequent models
R134a/5AlO (99/1) P_a = 0 W (file:ACOAL0.dat)	X_1,X_3 (190 of 194) 98 % X_1,X_2,X_3 (4 of 194) 2 %
R134a/5AlO (99/1) P_a = 4 W (file:ACOAL4.dat)	X_1,X_2,X_3 (129 of 243) 53 % X_1,X_2,X_5 (71 of 243) 29 % X_1,X_2,X_8 (28 of 243) 12 %
R134a/5AlO (99/1) P_a = 6 W (file:ACOAL6.dat)	X_1,X_2,X_3 (86 of 219) 39 % X_1,X_2,X_8 (73 of 219) 33 % X_1,X_2,X_5 (30 of 219) 14 %
R134a/5AlO (99/1) P_a = 8 W (file:ACOAL8.dat)	X_1,X_2,X_3 (185 of 248) 75 % X_1,X_2,X_5 (23 of 248) 9 % X_1,X_2,X_8 (18 of 248) 7 %
R134a/5AlO (99/1) P_a = 12 W (file:ACOAL12.dat)	X_1,X_2,X_3 (44 of 48) 92 % X_1,X_2,X_8 (3 of 48) 6 %

This publication is available free of charge from: http://dx.doi.org/10.6028/NIST.TN.1836

Table 2 Pool boiling data

R134a/5Al0 (99/1)
P_a = 0 W
File: Acoal0.dat

ΔT_s (K)	q'' (W/m^2)
5.63	103 666.
5.64	103 788.
5.65	103 756.
5.38	97 854.
5.39	97 969.
5.40	97 949.
5.14	92 304.
5.14	92 256.
5.14	92 319.
4.87	86 783.
4.87	86 819.
4.88	86 852.
4.60	81 204.
4.61	81 262.
4.60	81 291.
4.31	75 719.
4.30	75 806.
4.31	75 881.
4.03	70 526.
4.02	70 538.
4.03	70 583.
3.71	64 910.
3.71	64 930.
3.71	64 948.
3.42	59 762.
3.42	59 839.
3.42	59 828.
3.14	54 802.
3.15	54 865.
3.15	54 880.
2.87	49 997.
2.88	49 987.
2.87	49 960.
2.61	45 235.
2.60	45 174.
2.61	45 232.
2.34	40 575.
2.33	40 472.
2.33	40 473.
2.08	36 186.
2.07	36 138.
2.08	36 182.
1.83	31 956.
1.83	31 900.
1.83	31 884.
1.61	27 924.
1.58	27 780.
1.59	27 788.
1.35	23 952.
1.33	23 759.
1.32	23 723.
1.09	19 853.
1.08	19 660.
1.08	19 682.
0.87	16 250.
0.85	16 060.
5.76	105 157.
5.75	104 896.
5.75	104 784.
5.49	98 967.
5.49	99 015.
5.50	99 073.
5.24	93 588.
5.24	93719.
5.25	93 800.
4.98	88 015.
4.97	87 977.
4.98	87 927.
4.70	82 560.
4.70	82 585.
4.71	82 631.
4.43	76 910.
4.43	76 919.
4.43	76 962.
4.14	71 468.
4.13	71 588.
4.14	71 649.
3.86	66 426.
3.87	66 472.
3.87	66 544.
3.56	61 104.
3.55	61 082.
3.54	61 086.
3.24	56 026.
3.25	56 204.
3.25	56 305.
2.97	51 465.
2.98	51 531.
2.98	51 584.
2.69	46 658.
2.68	46 563.
2.69	46 563.
2.40	41 879.
2.39	41 832.
2.41	41 926.
2.15	37 448.
2.14	37 311.
2.15	37 432.
1.88	33 215.
1.87	33 022.
1.87	32 980.
1.68	29 241.
1.64	28 873.
1.64	28 840.
1.41	25 016.
5.92	104 185.
5.92	104 103.
5.92	104 024.
5.62	97 800.
5.62	97 916.
5.62	97 911.
5.33	92 443.
5.34	92 512.
5.34	92 565.
5.07	87 136.
5.07	87 225.
5.08	87 250.
4.79	81 720.
4.79	81 794.
4.79	81 761.
4.49	76 011.
4.49	76 083.
4.49	76 163.
4.20	70 716.
4.20	70 880.
4.21	70 889.
3.92	65 731.
3.93	65 826.
3.93	65 806.
3.63	60 562.
3.64	60 561.
3.63	60 460.
3.35	55 404.
3.35	55 438.
3.35	55 419.
3.07	50 390.
3.06	50 416.
3.07	50 412.
2.79	45 681.
2.78	45 542.
2.78	45 677.
2.51	41 033.
2.50	40 946.
2.50	40 943.
2.23	36 410.
2.22	36 234.
2.21	36 272.
1.95	32 013.
1.95	32 001.
5.67	104 441.
5.69	104 503.
5.70	104 449.
5.44	98 563.
5.45	98 712.
5.46	98 747.
5.20	93 199.
5.20	93 296.
5.21	93 403.
4.95	87 643.
4.94	87 563.
4.95	87 502.
4.66	81 944.
4.66	81 983.
4.66	82 007.
4.37	76 661.
4.38	76 689.
4.38	76 739.
4.10	71 371.
4.09	71 417.
4.10	71 424.
3.81	66 173.
3.81	66 138.
3.81	66 136.
3.53	60 969.
3.53	61 001.
3.54	61 090.

3.26	56 082.
3.25	56 000.
3.26	56 049.
2.98	51 030.
2.97	51 050.
2.97	51 014.
2.70	46 174.
2.69	46180.
2.70	46215.
2.44	41546.
2.43	41527.
2.44	41545.
2.17	37097.
2.16	37002.
2.16	37017.
1.90	32747.
1.89	32626.
1.89	32581.

R134a/5Al0 (99/1)
P_a = 4 W
File: Acoal4.dat

ΔT_s (K)	q'' (W/m^2)
5.66	103826.
5.67	104019.
5.67	103993.
5.39	97739.
5.38	97858.
5.39	97914.
5.11	92059.
5.11	92126.
5.12	92217.
4.85	86515.
4.85	86613.
4.86	86663.
4.57	81059.
4.56	81120.
4.58	81104.
4.31	75536.
4.31	75537.
4.31	75643.
4.02	70192.
4.03	70235.
4.02	70140.
3.74	64966.
3.75	65082.
3.76	65208.
3.48	59956.
3.49	59973.
3.49	59984.
3.21	54955.
3.20	54899.
3.21	54962.
2.93	50209.
2.93	50206.
2.93	50235.
2.68	45665.
2.68	45659.
2.67	45619.
2.42	41135.
2.41	41060.
2.41	41051.
2.15	36669.
2.14	36634.
2.14	36470.
1.89	32184.
1.87	32106.
1.87	32120.
1.63	28315.
1.62	28159.
1.63	28200.
1.39	24151.
1.36	23892.
1.36	23839.
1.12	20210.
1.10	20213.
5.69	102793.
5.69	102784.
5.68	102668.
5.40	96869.
5.40	96953.
5.40	97138.
5.11	91100.
5.12	91275.
5.13	91338.
4.85	85802.
4.84	85772.
4.86	85904.
4.58	80228.
4.58	80301.
4.59	80297.
4.31	74755.
4.30	74604.
4.30	74516.
4.01	69278.
4.03	69386.
4.03	69526.
3.77	64455.
3.77	64504.
3.76	64513.
3.49	59370.
3.49	59402.
3.49	59391.
3.22	54514.
3.21	54518.
3.21	54554.
2.95	49874.
2.94	49871.
2.94	49887.
2.69	45256.
2.68	45130.
2.68	45129.
2.42	40572.
2.41	40602.
2.41	40539.
2.16	36321.
2.14	36203.
2.14	36251.
1.89	32035.
1.87	31887.
1.86	31776.
1.62	27993.
1.61	27847.
1.61	27903.
1.36	23882.
5.48	102590.
5.48	102839.
5.48	102781.
5.20	96890.
5.20	96946.
5.21	97090.
4.94	91160.
4.94	91278.
4.94	91298.
4.68	85737.
4.68	85774.
4.68	85798.
4.41	80111.
4.41	80032.
4.13	74638.
4.14	74763.
4.14	74872.
3.89	69640.
3.88	69631.
3.87	69545.
3.60	64412.
3.61	64525.
3.61	64529.
3.34	59465.
3.34	59488.
3.34	59504.
3.07	54607.
3.07	54613.
3.08	54661.
2.82	49990.
2.81	49874.
2.82	49952.
2.56	45291.
2.56	45225.
2.57	45250.
2.30	40782.
2.30	40675.
2.30	40706.
5.63	103677.
5.63	103826.
5.63	103857.
5.35	97628.
5.36	97813.
5.35	97795.
5.08	91934.
5.08	92021.
5.08	92127.
4.81	86235.
4.80	86346.
4.81	86334.
4.55	80975.
4.54	81096.
4.55	81039.
4.28	75498.
4.27	75440.
4.27	75426.
3.99	70065.
4.00	70130.

This publication is available free of charge from: http://dx.doi.org/10.6028/NIST.TN.1836

3.99	70168.
3.72	64883.
3.72	64977.
3.72	64946.
3.45	59819.
3.45	59829.
3.45	59979.
3.19	54907.
3.17	54900.
3.18	54916.
2.92	50095.
2.92	50001.
2.91	50019.
2.66	45391.
2.64	45307.
2.65	45440.
2.38	40836.
2.38	40983.
2.38	40844.
2.12	36260.
2.10	36295.
2.10	36234.
1.86	32122.
1.85	32049.
1.85	32035.
1.61	28008.
1.59	27914.
1.60	27887.
1.36	23797.
1.33	23590.
1.33	23567.
1.14	20424.
1.11	20044.
5.52	105142.
5.53	105171.
5.54	105173.
5.28	99082.
5.28	99168.
5.30	99216.
5.04	93482.
5.05	93554.
5.07	93592.
4.80	87832.
4.80	87859.
4.81	87892.
4.54	82335.
4.54	82417.
4.54	82483.
4.27	76904.
4.26	76938.
4.27	77087.
3.99	71551.
4.00	71706.
4.00	71698.
3.72	66253.
3.72	66224.
3.72	66161.
3.43	60812.
3.42	60863.
3.43	60909.
3.15	55937.
3.15	55963.
3.15	56018.
2.88	51008.
2.88	50986.
2.88	50950.
2.61	46159.
2.60	46036.
2.59	46074.
2.33	41496.
2.33	41458.
2.33	41472.
2.07	37076.
2.07	36996.
2.06	36955.
1.81	32548.
1.80	32416.
1.80	32300.
1.57	28252.
1.54	28053.
1.55	28363.
1.33	24466.
1.32	24341.

R134a/5Al0 (99/1)
P_a = 6 W
File: Acoal6.dat

ΔT_s (K)	q'' (W/m^2)
5.35	104525.
5.36	104562.
5.36	104756.
5.09	98646.
5.10	98854.
5.11	98861.
4.85	92980.
4.86	93089.
4.86	93046.
4.60	87212.
4.60	87305.
4.60	87272.
4.35	81854.
4.36	81876.
4.36	81969.
4.10	76348.
4.10	76399.
4.11	76480.
3.84	71076.
3.84	71165.
3.85	71207.
3.57	65722.
3.57	65783.
3.58	65798.
3.31	60751.
3.31	60720.
3.31	60702.
3.04	55487.
3.03	55625.
3.03	55666.
2.77	50642.
2.79	50688.
2.78	50707.
2.54	46425.
2.53	46540.
2.54	46319.
2.27	41843.
2.27	41761.
2.27	41792.
2.02	37399.
2.00	37205.
2.00	37129.
1.76	32789.
1.74	32675.
1.74	32753.
1.51	28817.
1.50	28537.
5.28	105131.
5.29	105124.
5.29	105233.
5.04	99299.
5.04	99480.
5.06	99638.
4.79	93668.
4.80	93840.
4.81	93836.
4.56	88080.
4.57	88163.
4.58	88349.
4.31	82568.
4.31	82685.
4.31	82690.
4.05	76952.
4.05	76991.
4.05	77036.
3.79	71752.
3.79	71828.
3.79	71755.
3.53	66284.
3.51	66412.
3.52	66477.
3.25	61339.
3.25	61235.
3.25	61240.
2.98	56244.
2.99	56152.
2.99	56121.
2.73	51419.
2.74	51465.
2.75	51497.
2.49	46809.
2.48	46801.
2.48	46783.
2.22	42244.
2.22	42193.
2.23	42178.
1.98	37506.
1.97	37490.
1.96	37490.
1.73	33196.
1.71	33081.
1.72	33038.
1.47	28703.
1.46	28766.
1.45	28494.
1.24	24858.

This publication is available free of charge from: http://dx.doi.org/10.6028/NIST.TN.1836

1.23	24651.
1.22	24549.
1.01	20883.
0.98	20609.
0.98	20549.
0.79	17099.
0.76	16827.
5.32	105406.
5.31	105441.
5.32	105523.
5.07	99230.
5.07	99332.
5.07	99400.
4.83	93499.
4.84	93698.
4.84	93786.
4.59	87711.
4.58	87817.
4.59	87885.
4.34	82296.
4.34	82346.
4.34	82345.
4.08	76796.
4.08	77011.
4.09	77107.
3.83	71567.
3.83	71609.
3.83	71591.
3.56	66343.
3.56	66410.
3.57	66445.
3.30	60938.
3.29	61086.
3.29	61063.
3.04	56249.
3.03	56195.
3.04	56336.
2.80	51518.
2.78	51346.
2.78	51370.
2.53	46774.
2.52	46708.
2.52	46708.
2.25	42152.
2.22	42163.
2.26	42103.
2.01	37404.
1.99	37365.
1.99	37324.
1.74	33037.
1.72	32938.
1.72	33024.
1.47	28866.
1.45	28677.
1.45	28682.
1.21	24544.
1.18	24435.
1.18	24297.
0.97	20567.
0.92	20221.
0.92	20479.
0.73	17183.

0.70	16827.
0.69	16671.
0.48	13197.
0.46	12889.
5.23	105953.
5.23	106049.
5.22	105864.
4.97	99583.
4.97	99680.
4.98	99774.
4.73	93675.
4.73	93711.
4.73	93792.
4.48	87964.
4.49	87993.
4.49	87881.
4.23	82289.
4.24	82348.
4.23	82383.
3.98	76727.
3.98	76730.
3.98	76740.
3.72	71390.
3.72	71449.
3.73	71488.
3.48	66196.
3.47	66173.
3.47	66192.
3.19	61026.
3.20	61132.
3.19	61055.
2.94	56077.
2.93	56065.
2.94	56106.
2.70	51520.
2.69	51464.
2.71	51478.
2.45	46789.
2.45	46702.
2.45	46717.
2.19	42132.
2.19	42105.
2.20	42138.
1.96	37593.
1.94	37546.
1.94	37536.
1.69	33144.
1.68	33011.
1.68	32892.
1.44	28881.
1.44	28776.
1.43	28681.
1.19	24498.
1.18	24216.
1.18	24135.
0.95	20575.
0.94	20433.
0.94	20434.
0.74	16984.
0.71	16719.
0.71	16632.

R134a/5Al0 (99/1)
P_a = 8 W
File: Acoal8.dat

ΔT_s (K)	q'' (W/m^2)
5.29	105740.
5.31	105741.
5.30	105581.
5.04	99211.
5.05	99241.
5.05	99263.
4.80	93162.
4.80	93144.
4.81	93293.
4.55	87376.
4.55	87466.
4.56	87498.
4.31	82018.
4.31	82050.
4.31	82080.
4.05	76404.
4.05	76409.
4.05	76400.
3.79	71041.
3.79	71109.
3.79	71129.
3.53	65784.
3.52	65779.
3.52	65734.
3.26	60695.
3.25	60699.
3.26	60750.
2.99	55673.
2.99	55667.
2.98	55664.
2.72	50889.
2.72	50992.
2.73	51013.
2.47	46197.
2.47	46136.
2.46	46119.
2.20	41501.
2.20	41467.
2.21	41469.
1.96	37053.
1.95	36981.
1.95	36985.
1.71	32725.
1.70	32651.
1.70	32658.
1.46	28364.
1.45	28253.
1.45	28192.
1.24	24427.
1.23	24431.
1.21	24066.
1.01	20817.
0.98	20481.
0.98	20298.

This publication is available free of charge from: http://dx.doi.org/10.6028/NIST.TN.1836

0.78	16891.
0.75	16617.
5.70	104169.
5.70	104138.
5.70	104169.
5.41	98168.
5.42	98473.
5.43	98738.
5.16	93033.
5.17	93240.
5.18	93338.
4.91	87429.
4.91	87619.
4.91	87677.
4.61	81603.
4.62	81586.
4.61	81587.
4.33	75947.
4.32	76069.
4.33	76066.
4.05	70729.
4.06	70834.
4.07	70815.
3.78	65531.
3.78	65577.
3.79	65616.
3.49	60322.
3.50	60305.
3.50	60325.
3.23	55173.
3.22	55145.
3.22	55170.
2.94	50364.
2.94	50421.
2.94	50438.
2.65	45666.
2.66	45599.
2.67	45642.
2.40	41032.
2.40	40977.
2.40	41017.
2.12	36682.
2.12	36602.
2.12	36644.
1.86	32055.
1.85	32207.
1.85	32199.
1.60	28072.
1.59	28150.
1.59	28171.
1.37	24480.
5.49	105143.
5.50	105339.
5.50	105418.
5.24	99079.
5.27	99304.
5.27	99442.
5.01	93537.
5.02	93609.
5.03	93770.
4.76	87891.
4.76	87963.

4.77	88023.
4.49	82363.
4.49	82630.
4.51	82747.
4.24	76978.
4.24	76950.
4.24	76975.
3.94	71403.
3.95	71582.
3.96	71633.
3.68	66310.
3.67	66316.
3.68	66266.
3.38	61045.
3.39	61072.
3.39	61111.
3.11	56170.
3.09	56143.
3.10	56175.
2.83	51191.
2.82	51188.
2.82	51204.
2.53	46338.
2.51	46229.
2.51	46205.
2.27	41730.
2.27	41734.
2.27	41785.
2.02	37387.
2.02	37287.
2.01	37209.
1.76	32860.
1.75	32870.
1.76	32808.
1.52	28827.
1.51	28730.
1.50	28421.
1.30	24945.
5.37	105619.
5.39	105803.
5.39	105873.
5.14	99655.
5.15	99831.
5.16	99952.
4.89	93937.
4.91	94119.
4.92	94288.
4.66	88227.
4.66	88371.
4.67	88413.
4.40	82686.
4.40	82842.
4.41	82873.
4.13	77230.
4.13	77312.
4.14	77349.
3.86	71730.
3.86	71768.
3.86	71832.
3.58	66394.
3.58	66410.
3.58	66422.

3.32	61392.
3.31	61396.
3.32	61393.
3.05	56307.
3.05	56257.
3.05	56119.
2.77	51226.
2.77	51224.
2.77	51269.
2.51	46573.
2.51	46505.
2.50	46387.
2.24	41738.
2.24	41774.
2.24	41745.
1.99	37320.
1.98	37258.
1.98	37197.
1.75	33021.
1.73	32927.
1.73	32941.
1.55	28745.
1.53	28570.
1.53	28495.
1.30	24540.
5.37	105586.
5.40	105650.
5.41	105501.
5.14	99100.
5.15	99230.
5.16	99315.
4.93	93549.
4.94	93563.
4.95	93598.
4.69	87844.
4.69	87838.
4.70	87972.
4.45	82570.
4.45	82677.
4.46	82711.
4.18	77113.
4.18	77164.
4.17	77150.
3.90	71636.
3.91	71717.
3.91	71755.
3.63	66308.
3.62	66349.
3.63	66346.
3.34	61047.
3.35	61122.
3.35	61168.
3.07	56152.
3.08	56157.
3.08	56181.
2.81	51049.
2.80	51087.
2.81	51133.
2.55	46333.
2.54	46288.
2.54	46274.
2.29	41617.

This publication is available free of charge from: http://dx.doi.org/10.6028/NIST.TN.1836

2.29	41526.
2.29	41608.
2.04	37194.
2.03	37238.
2.02	37220.
1.80	32808.
1.77	32612.
1.77	32542.

R134a/5Al0 (99/1)
P_a = 12 W
File: Acoal12.dat

ΔT_s	q''
3.16	55701.
3.16	55710.
3.15	55729.
2.88	50751.
2.88	50815.
2.88	50778.
2.61	46082.
2.60	45939.
2.61	45961.
2.35	41405.
2.33	41372.
2.33	41377.
2.08	37112.
2.07	37004.
2.07	36778.
1.81	32399.
1.80	32319.
1.79	32321.
1.58	28519.
1.56	28319.
1.55	28295.

(K)	(W/m^2)
5.41	105116.
5.42	105234.
5.43	105156.
5.19	98932.
5.20	99014.
5.22	99003.
4.98	93199.
4.99	93202.
5.00	93116.
4.75	87427.
4.76	87440.
4.77	87536.
4.50	81883.
4.50	81922.
4.51	81980.

4.24	76430.
4.24	76454.
4.25	76463.
3.98	70911.
3.97	70942.
3.97	70946.
3.71	65805.
3.71	65856.
3.71	65857.
3.43	60723.
3.44	60683.
3.44	60680.

This publication is available free of charge from: http://dx.doi.org/10.6028/NIST.TN.1836

Table 3 Number of test days and data points

Fluid (% mass fraction)	Number of days	Number of data points
R134a/5AlO (99/1) P_a = 0 W 0.8 K ≤ ΔT_s ≤ 5.8 K	4	194
R134a/5AlO (99/1) P_a = 4 W 1. 1 K ≤ ΔT_s ≤ 5.6 K	5	243
R134a/5AlO (99/1) P_a = 6 W 0.4 K ≤ ΔT_s ≤ 5.3 K	4	219
R134a/5AlO (99/1) P_a = 8 W 0.8 K ≤ ΔT_s ≤ 5.4 K	5	248
R134a/5AlO (99/1) P_a = 12 W 1.0 K ≤ ΔT_s ≤ 6.0 K	1	48

This publication is available free of charge from: http://dx.doi.org/10.6028/NIST.TN.1836

Table 4 Estimated parameters for cubic boiling curve fits for Turbo-BII-HP copper surface

$\Delta T_s = A_0 + A_1 q'' + A_2 q''^2 + A_3 q''^3$

ΔT_s in kelvin and q'' in W/m^2

Fluid	A_o	A_1	A_2	A_3
R134a/5AlO (99/1) P_a = 0 W 0.8 K ≤ ΔT_s ≤ 5.8 K	-0.150578	6.32198×10^{-5}	-1.36492×10^{-12}	-6.03840×10^{-16}
R134a/5AlO (99/1) P_a = 4 W 1. 1 K ≤ ΔT_s ≤ 5.6 K	-0.158376	6.45856×10^{-5}	-5.78231×10^{-11}	-3.01352×10^{-16}
R134a/5AlO (99/1) P_a = 6 W 0.4 K ≤ ΔT_s ≤ 5.3 K	-0.375243	6.75659×10^{-5}	-1.26793×10^{-10}	-3.30088×10^{-17}
R134a/5AlO (99/1) P_a = 8 W 0.8 K ≤ ΔT_s ≤ 5.4 K	-0.197504	5.97647×10^{-5}	3.29158×10^{-11}	-8.80686×10^{-16}
R134a/5AlO (99/1) P_a = 12 W 1.0 K ≤ ΔT_s ≤ 6.0 K	-0.111051	5.68618×10^{-5}	1.15503×10^{-10}	-1.48576×10^{-15}

This publication is available free of charge from: http://dx.doi.org/10.6028/NIST.TN.1836

Table 5 Residual standard deviation of ΔT_s

Fluid	(K)
R134a/5AlO (99/1) P_a = 0 W 0.8 K ≤ ΔT_s ≤ 5.8 K	0.06
R134a/5AlO (99/1) P_a = 4 W 1. 1 K ≤ ΔT_s ≤ 5.6 K	0.06
R134a/5AlO (99/1) P_a = 6 W 0.4 K ≤ ΔT_s ≤ 5.3 K	0.04
R134a/5AlO (99/1) P_a = 8 W 0.8 K ≤ ΔT_s ≤ 5.4 K	0.09
R134a/5AlO (99/1) P_a = 12 W 1.0 K ≤ ΔT_s ≤ 6.0 K	0.006

This publication is available free of charge from: http://dx.doi.org/10.6028/NIST.TN.1836

Table 6 Average magnitude of 95 % multi-use confidence interval for mean ΔT_s

Fluid	U (K)
R134a/5AlO (99/1) P_a = 0 W 0.8 K ≤ ΔT_s ≤ 5.8 K	0.03
R134a/5AlO (99/1) P_a = 4 W 1. 1 K ≤ ΔT_s ≤ 5.6 K	0.02
R134a/5AlO (99/1) P_a = 6 W 0.4 K ≤ ΔT_s ≤ 5.3 K	0.02
R134a/5AlO (99/1) P_a = 8 W 0.8 K ≤ ΔT_s ≤ 5.4 K	0.04
R134a/5AlO (99/1) P_a = 12 W 1.0 K ≤ ΔT_s ≤ 6.0 K	0.04

This publication is available free of charge from: http://dx.doi.org/10.6028/NIST.TN.1836

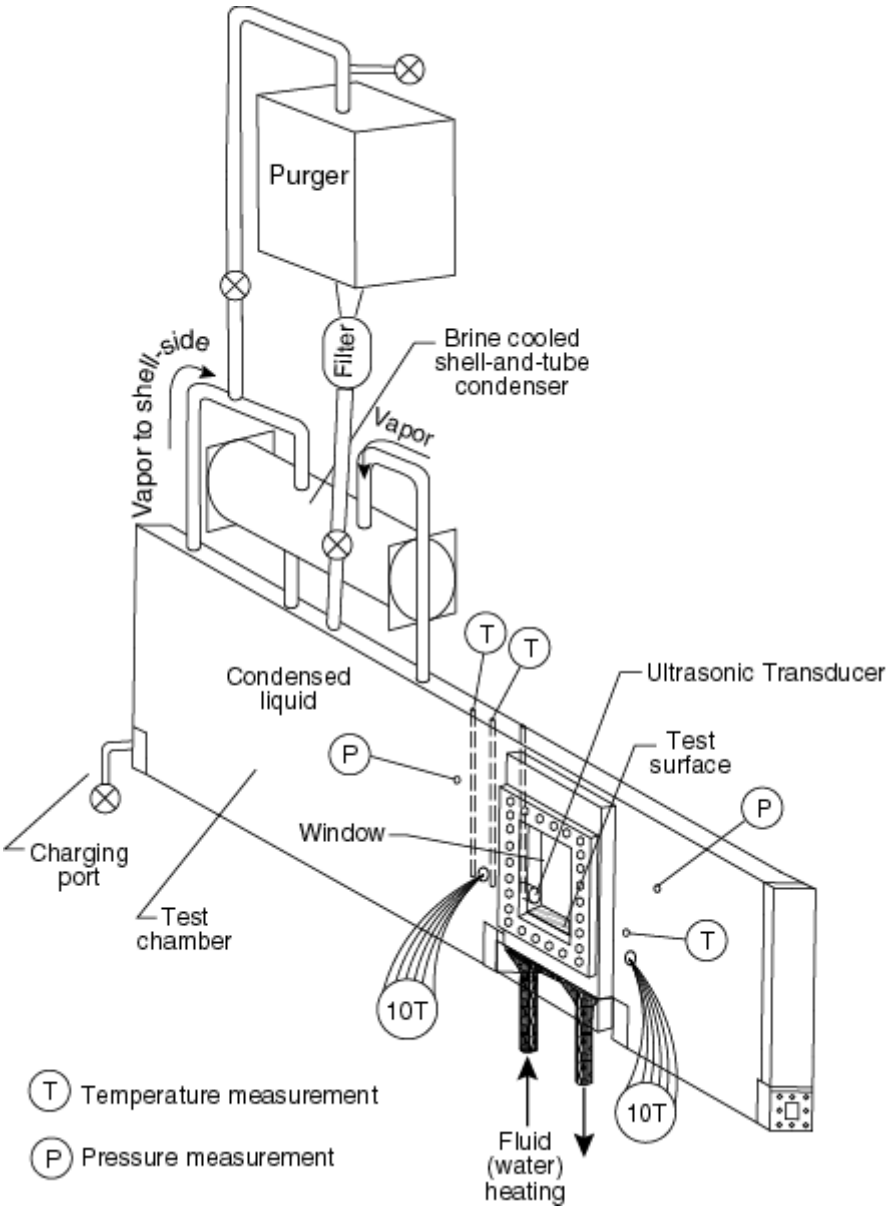

Fig. 1 Schematic of test apparatus

This publication is available free of charge from: http://dx.doi.org/10.6028/NIST.TN.1836

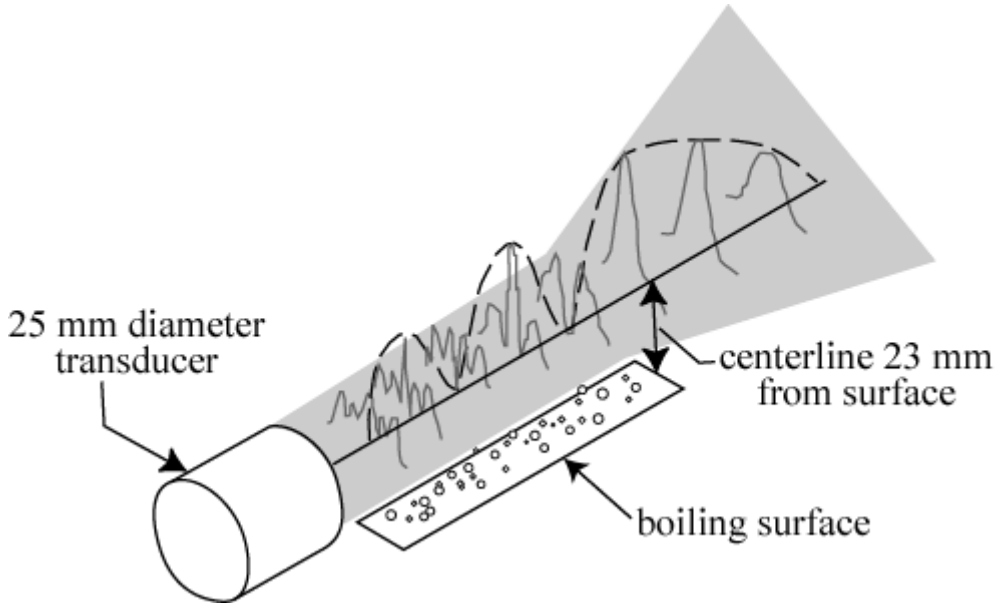

Fig. 2 Schematic of ultrasonic piezoelectric transducer showing presumed amplitude variations with respect to the boiling surface

This publication is available free of charge from: http://dx.doi.org/10.6028/NIST.TN.1836

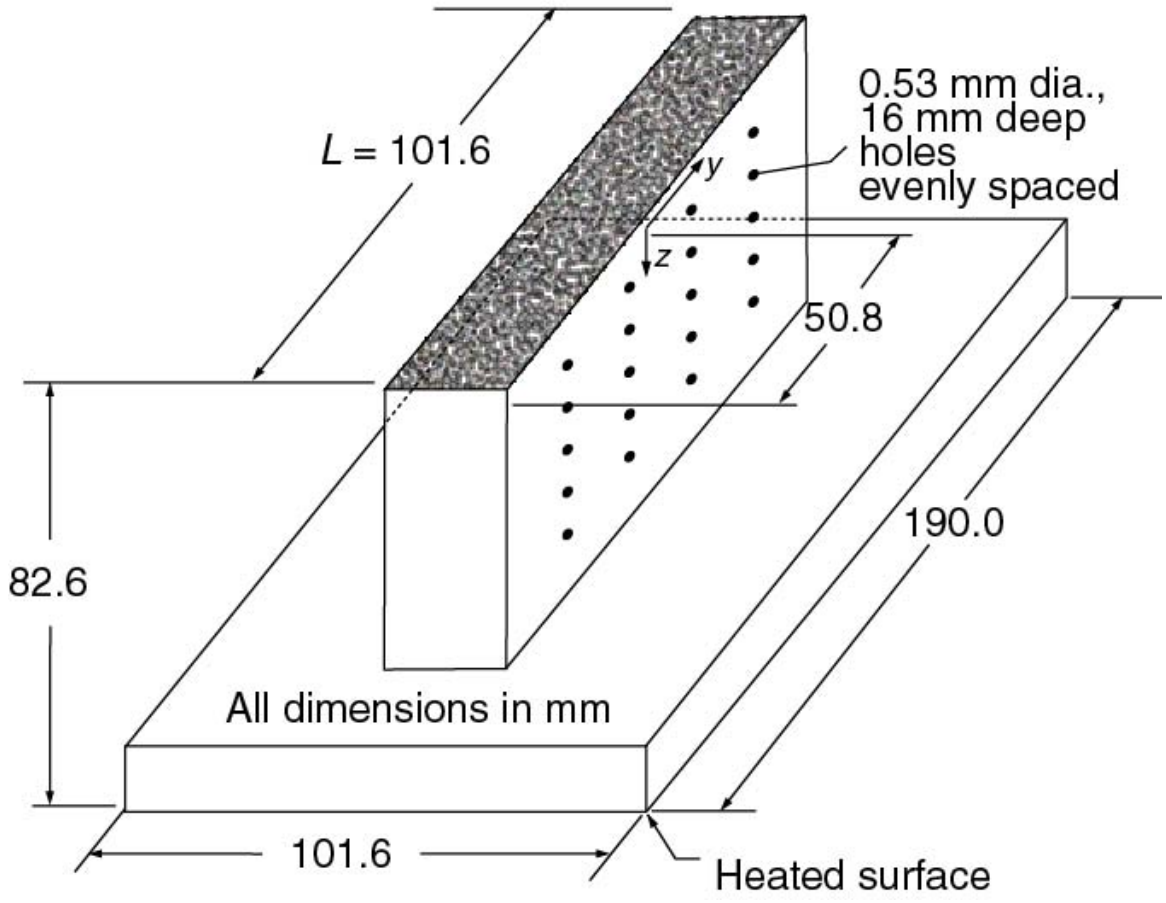

Fig. 3 OFHC copper flat test plate with Turbo-BII-HP surface and thermocouple coordinate system

This publication is available free of charge from: http://dx.doi.org/10.6028/NIST.TN.1836

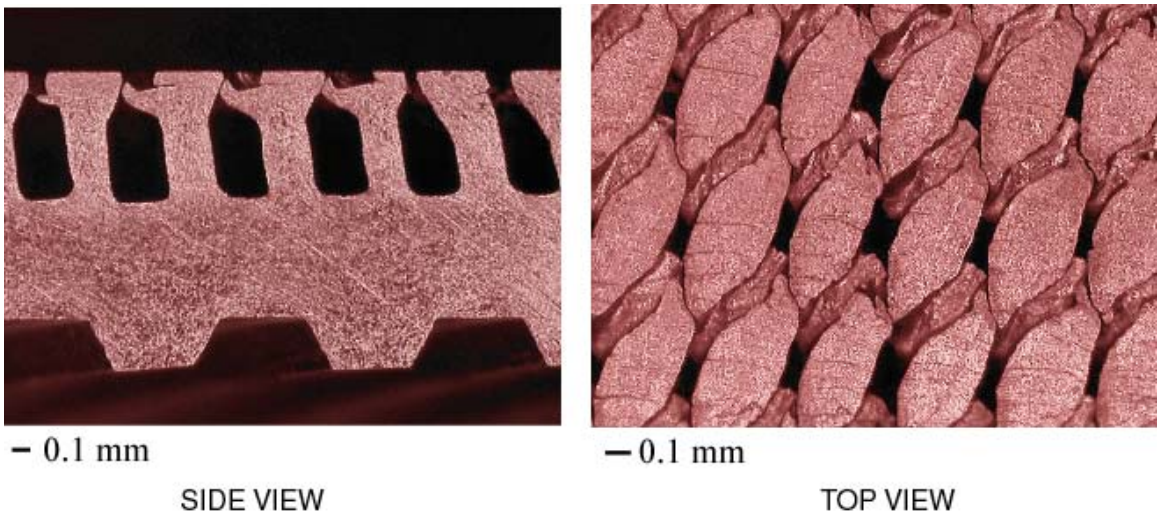

Fig. 4 Photograph of Turbo-BII-HP surface

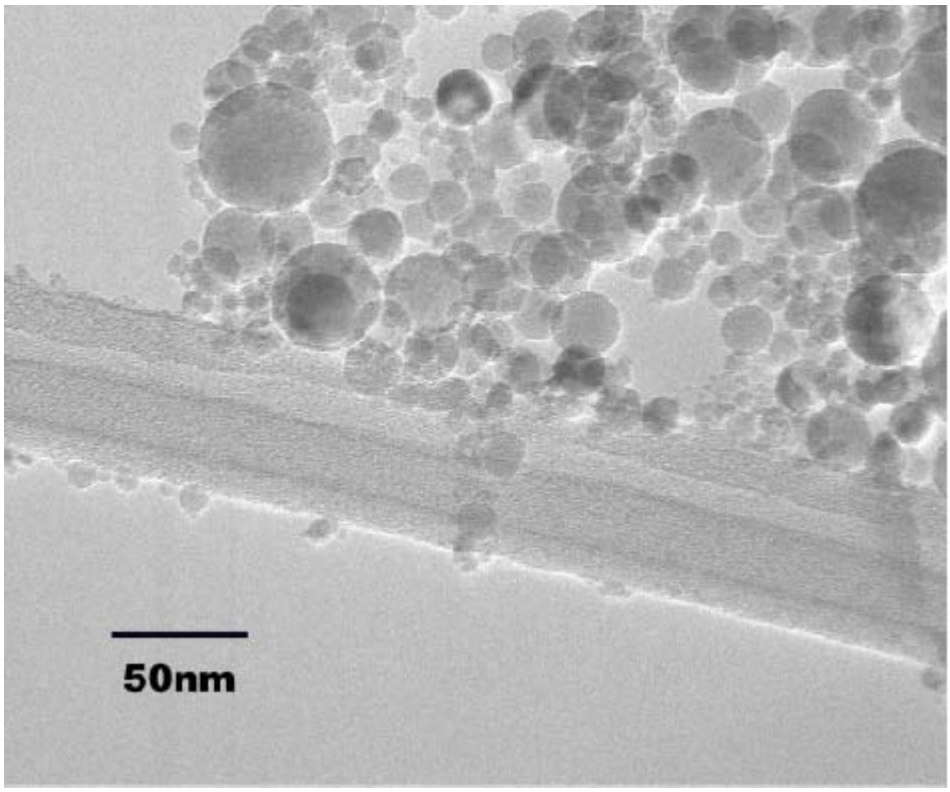

Fig. 5 TEM image of Al_2O_3 nanolubricant (Sarkas, 2009)

This publication is available free of charge from: http://dx.doi.org/10.6028/NIST.TN.1836

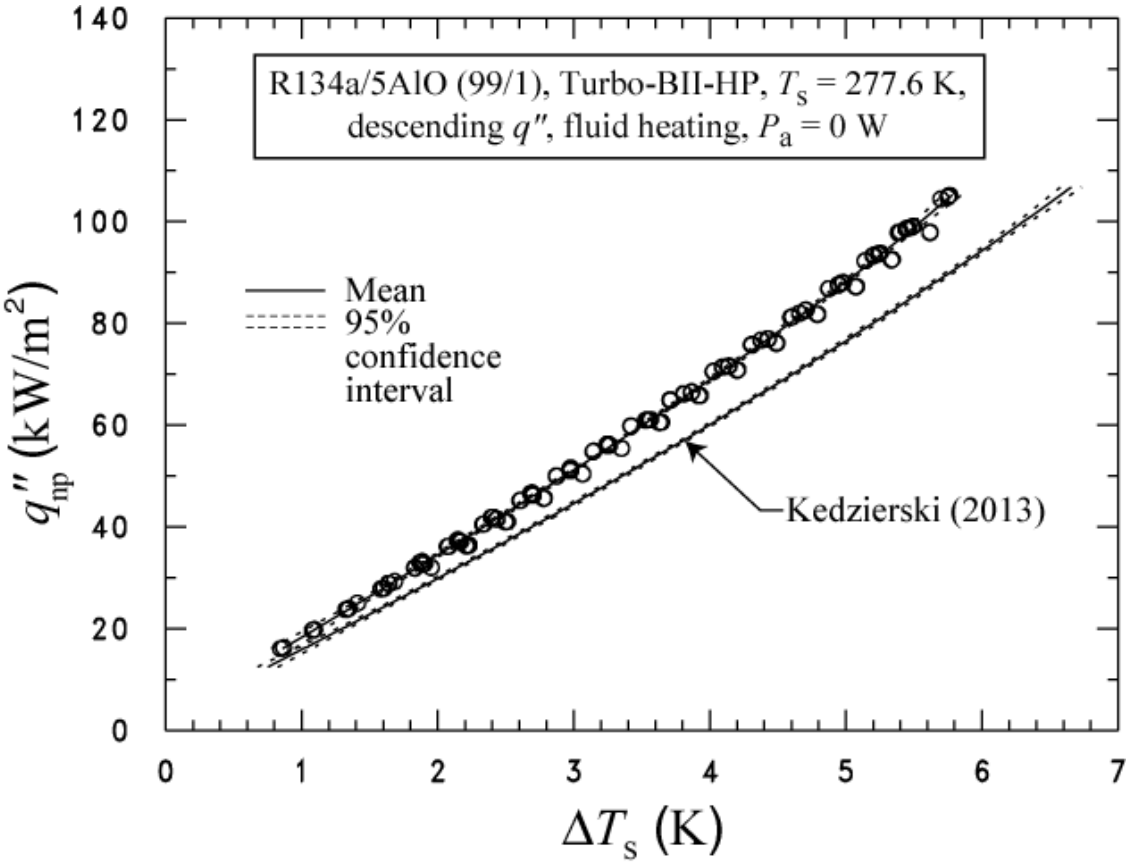

Fig. 6 R134a/5AlO (99/1) mixture boiling curves for Turbo-BII-HP and *P* = 0 W

This publication is available free of charge from: http://dx.doi.org/10.6028/NIST.TN.1836

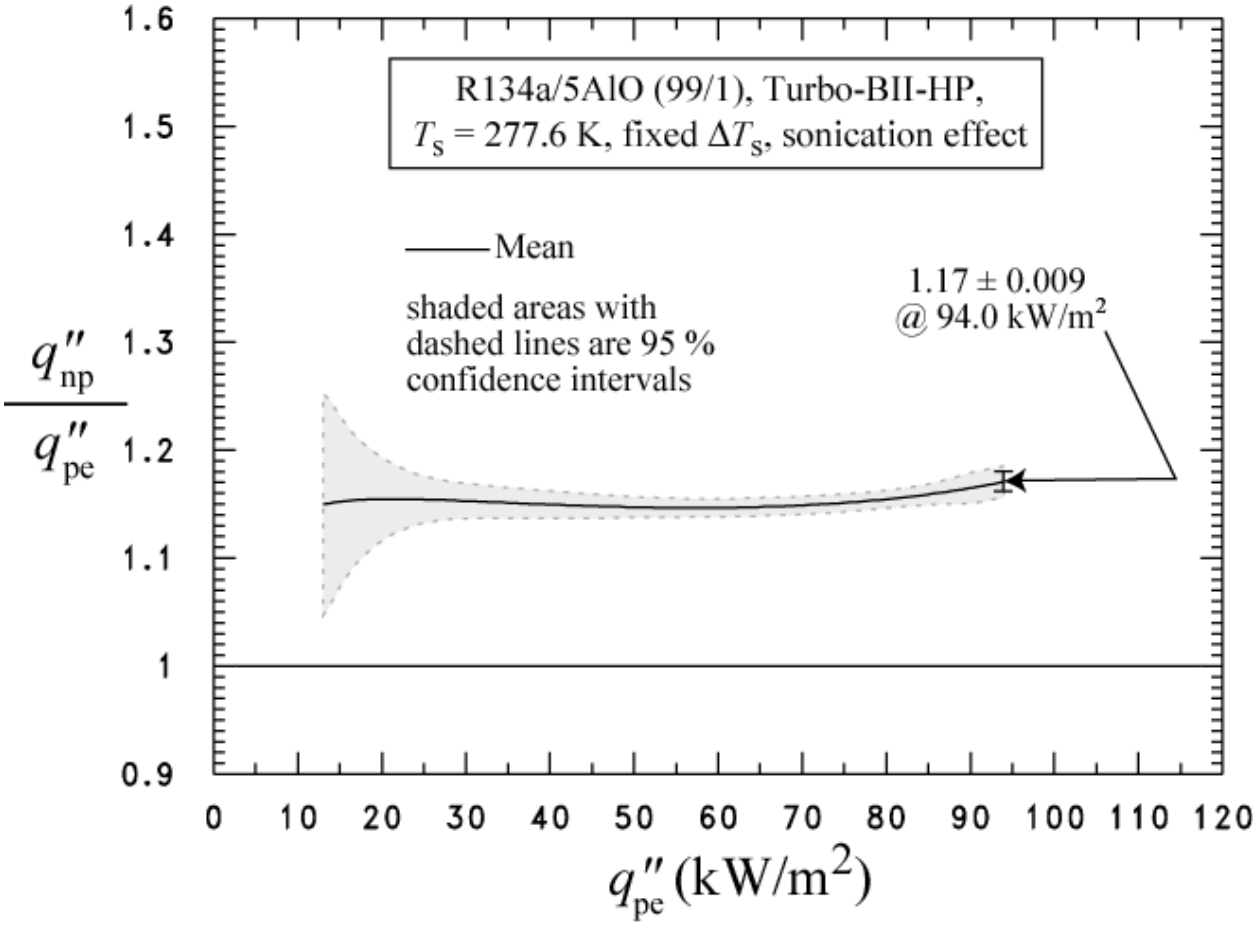

Fig. 7 Effect of extended acoustic excitation on the boiling heat flux of R134a/5ALO (99/1) Turbo-BII-HP

This publication is available free of charge from: http://dx.doi.org/10.6028/NIST.TN.1836

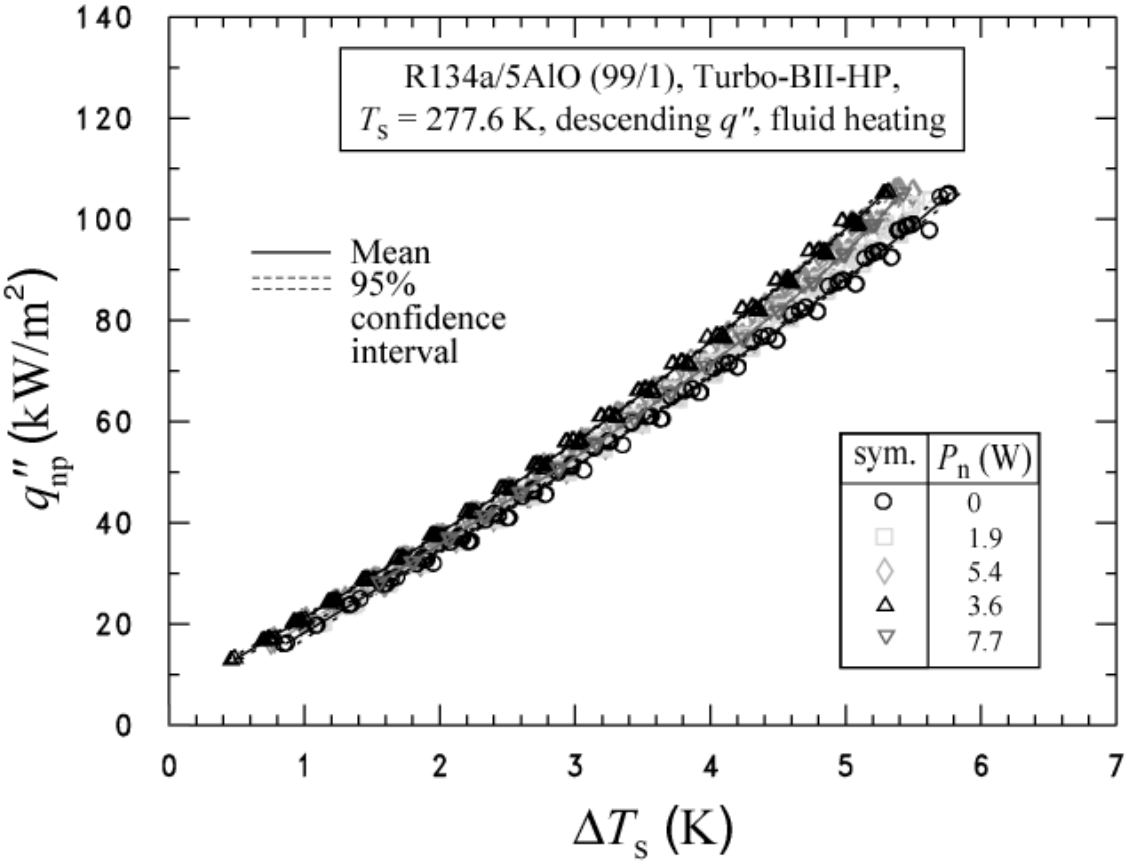

Fig. 8 R134a/nanolubricant mixtures boiling curves for Turbo-BII-HP for various ultrasonic applied levels

This publication is available free of charge from: http://dx.doi.org/10.6028/NIST.TN.1836

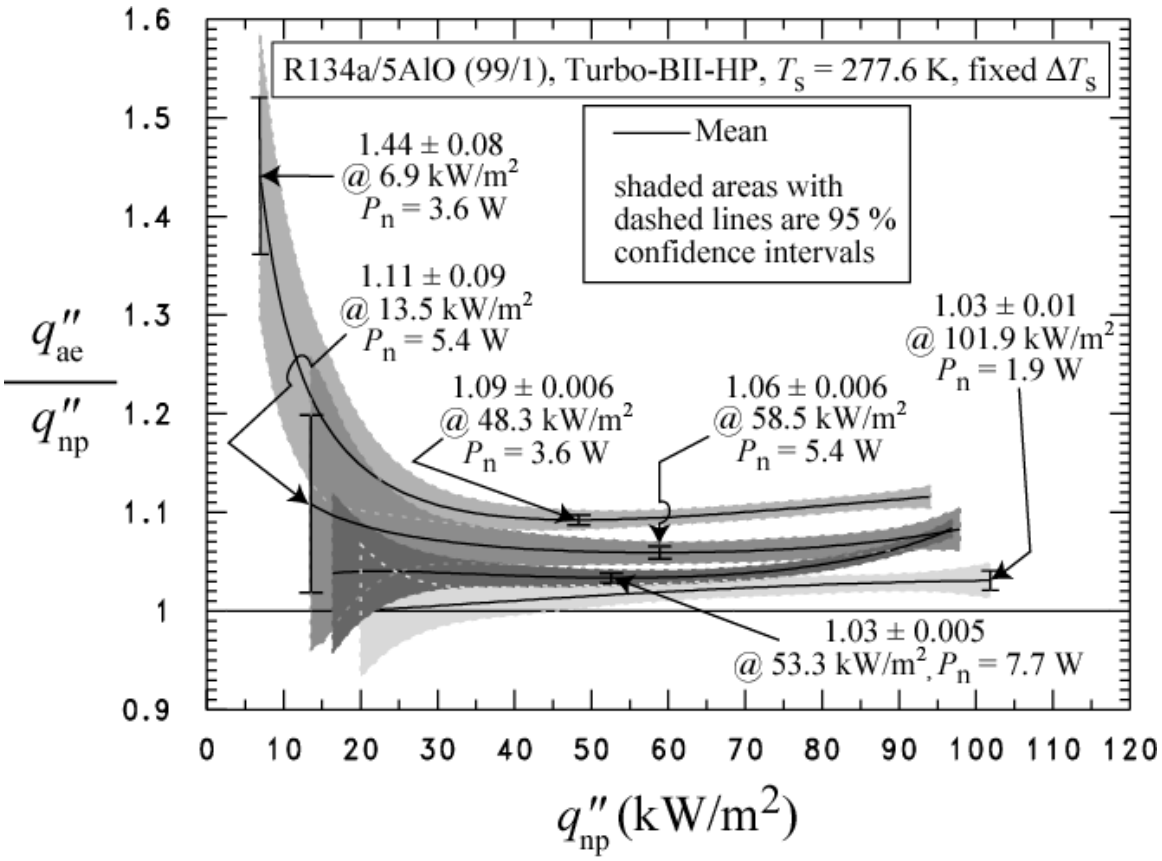

Fig. 9 Acoustically excited boiling heat flux of R134a/nanolubricant mixtures relative to that without excitation for Turbo-BII-HP

This publication is available free of charge from: http://dx.doi.org/10.6028/NIST.TN.1836

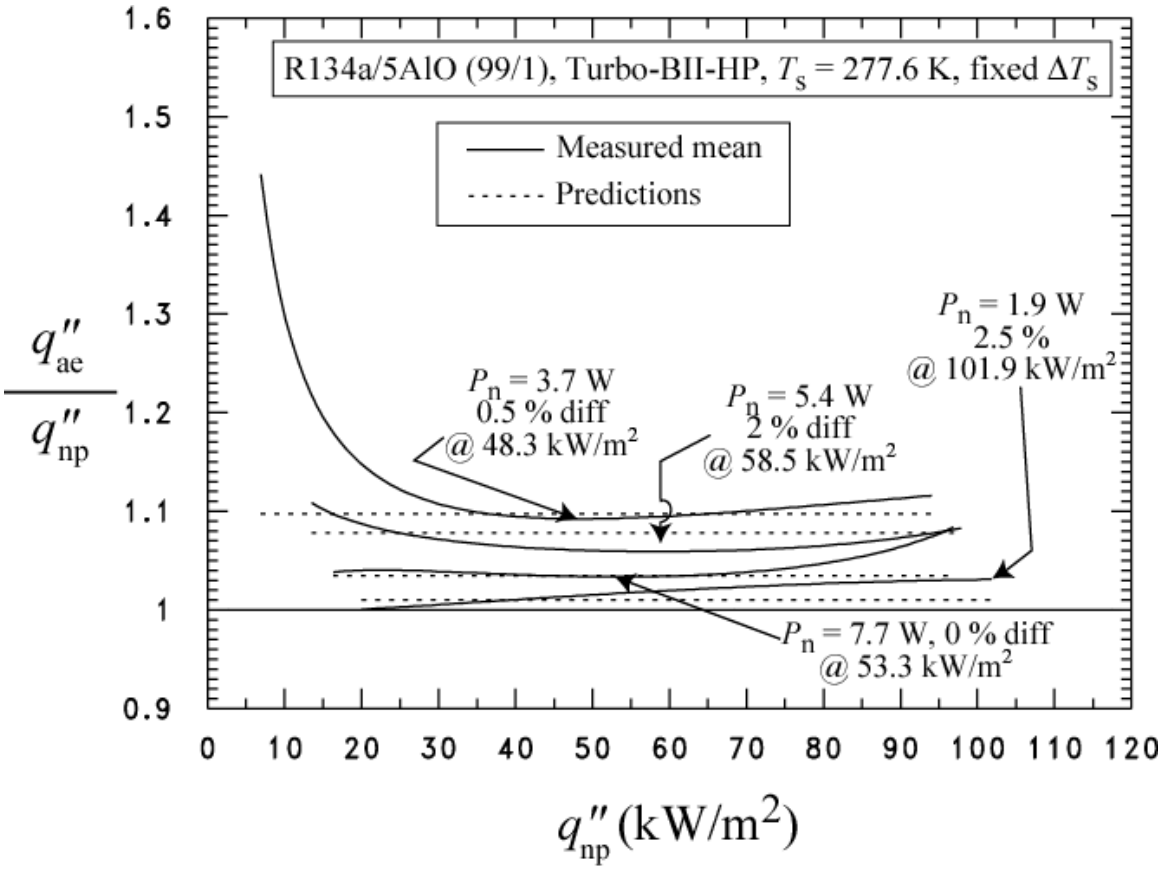

Fig. 10 Prediction of acoustically excited boiling heat flux of R134a/nanolubricant mixture relative for Turbo-BII-HP

This publication is available free of charge from: http://dx.doi.org/10.6028/NIST.TN.1836

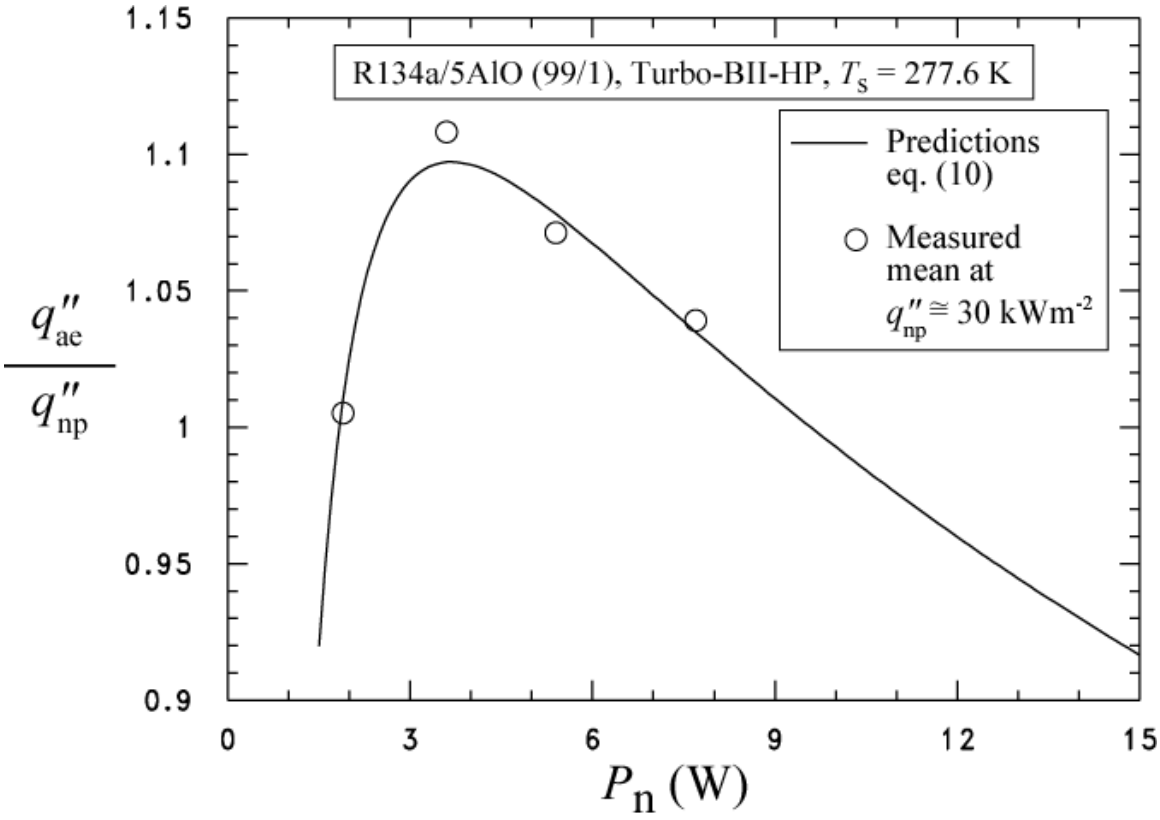

Fig. 11 Effect of net power on acoustically excited boiling heat flux of a R134a/nanolubricant mixture

This publication is available free of charge from: http://dx.doi.org/10.6028/NIST.TN.1836

APPENDIX A: UNCERTAINTIES

Figure A.1 shows the relative (percent) uncertainty of the heat flux ($U_{q''}$) as a function of the heat flux. Figure A.2 shows the uncertainty of the wall temperature as a function of the heat flux. The uncertainties shown in Figs. A.1 and A.2 are "within-run uncertainties." These do not include the uncertainties due to "between-run effects" or differences observed between tests taken on different days. The "within-run uncertainties" include only the random effects and uncertainties associated with one particular test. All other uncertainties reported in this study are "between-run uncertainties" which include all random effects such as surface past history or seeding.

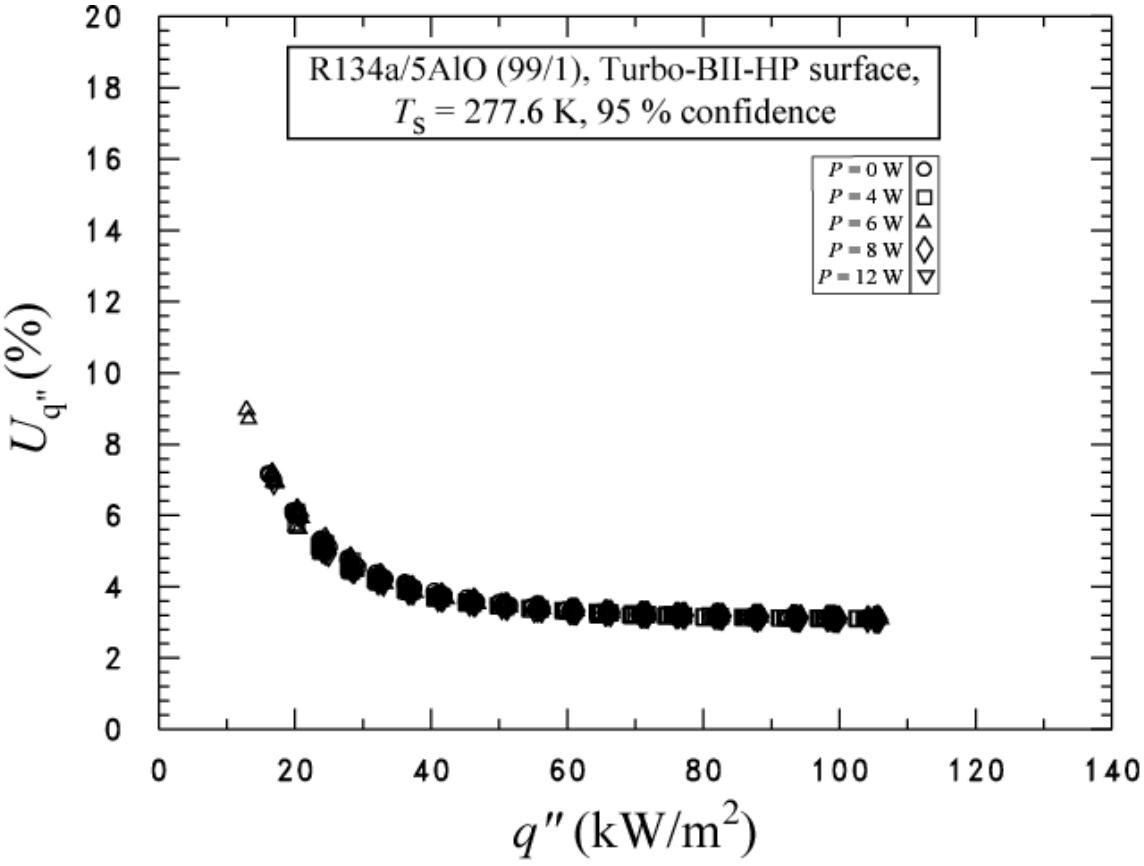

Fig. A.1 Expanded relative uncertainty in the heat flux of the surface at the 95 % confidence level

This publication is available free of charge from: http://dx.doi.org/10.6028/NIST.TN.1836

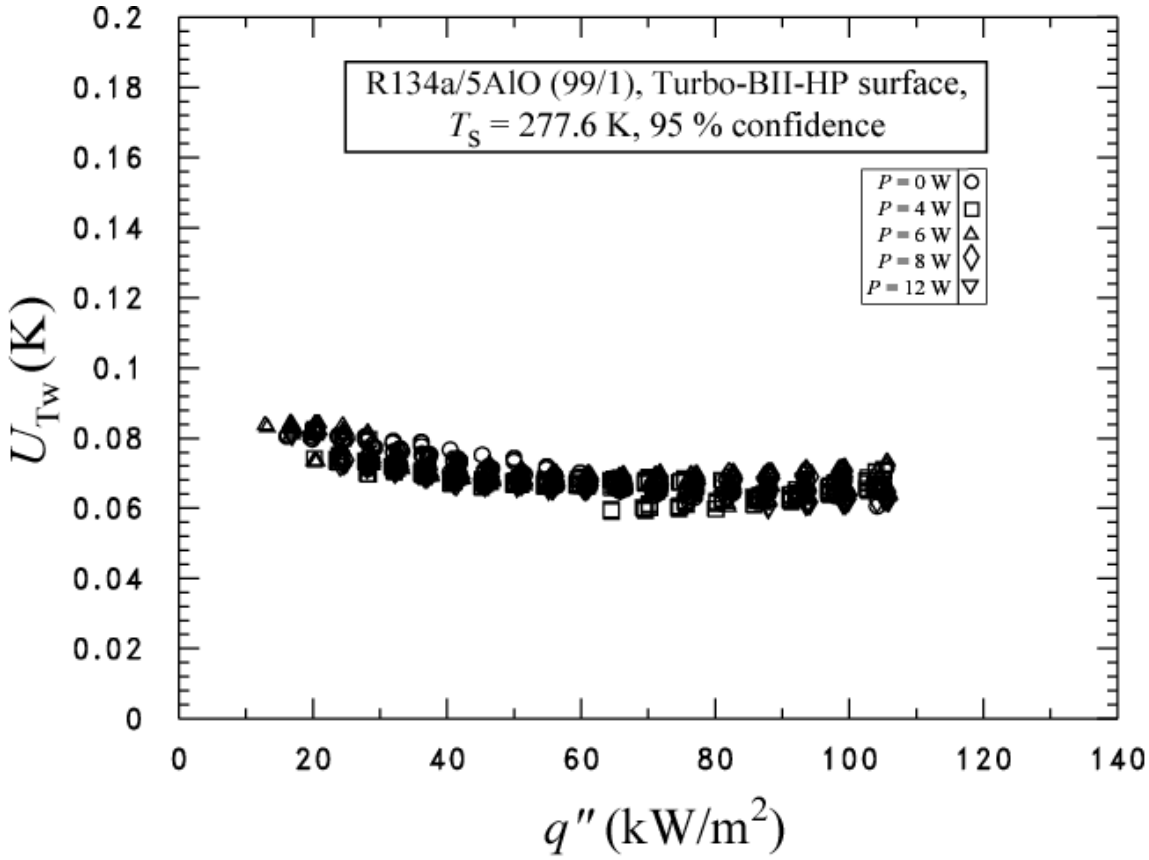

Fig. A.2 Expanded uncertainty in the temperature of the surface at the 95 % confidence level